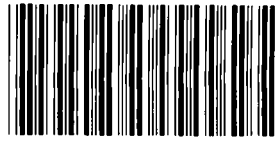


SANDIA REPORT

SAND92-1303 • UC-721

Unlimited Release

Printed October 1992



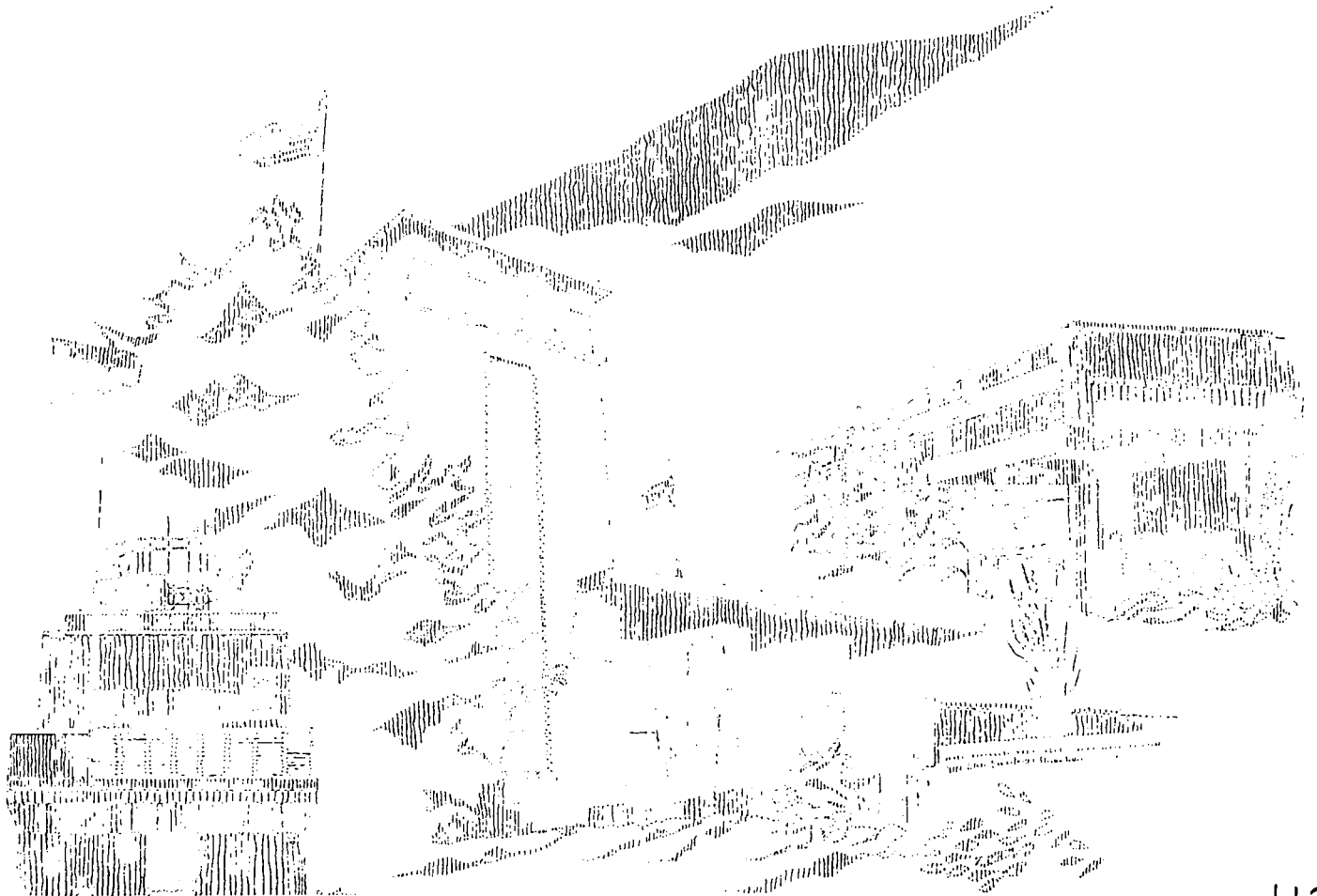
8533890

SANDIA NATIONAL
LABORATORIES
TECHNICAL LIBRARY

Exact Analysis of a Two-Dimensional Model for Brine Flow to a Borehole in a Disturbed Rock Zone

Fred Gelbard

Prepared by
Sandia National Laboratories
Albuquerque, New Mexico 87185 and Livermore, California 94550
for the United States Department of Energy
under Contract DE-AC04-76DP00789



Issued by Sandia National Laboratories, operated for the United States Department of Energy by Sandia Corporation.

NOTICE: This report was prepared as an account of work sponsored by an agency of the United States Government. Neither the United States Government nor any agency thereof, nor any of their employees, nor any of their contractors, subcontractors, or their employees, makes any warranty, express or implied, or assumes any legal liability or responsibility for the accuracy, completeness, or usefulness of any information, apparatus, product, or process disclosed, or represents that its use would not infringe privately owned rights. Reference herein to any specific commercial product, process, or service by trade name, trademark, manufacturer, or otherwise, does not necessarily constitute or imply its endorsement, recommendation, or favoring by the United States Government, any agency thereof or any of their contractors or subcontractors. The views and opinions expressed herein do not necessarily state or reflect those of the United States Government, any agency thereof or any of their contractors.

Printed in the United States of America. This report has been reproduced directly from the best available copy.

Available to DOE and DOE contractors from
Office of Scientific and Technical Information
PO Box 62
Oak Ridge, TN 37831

Prices available from (615) 576-8401, FTS 626-8401

Available to the public from
National Technical Information Service
US Department of Commerce
5285 Port Royal Rd
Springfield, VA 22161

NTIS price codes
Printed copy: A06
Microfiche copy: A01

Exact Analysis of a Two-Dimensional Model for Brine Flow to a Borehole in a Disturbed Rock Zone

Fred Gelbard
Fluid Flow and Transport Department 6119
Sandia National Laboratories
PO Box 5800
Albuquerque, NM 87185

ABSTRACT

An exact two-dimensional solution is derived for determining the fluid flow rates into a borehole and to the surface from which the borehole was drilled. The solution is for a single fluid phase in a disturbed rock zone (DRZ) that surrounds the borehole with a radius specified to be either finite or infinite. The solution is restricted to constant homogeneous rock and fluid properties in the DRZ, and pressures in the borehole and at the surface of the drift that are maintained constant at ambient conditions. A major objective of the work is to provide a benchmark for more detailed numerical calculations that include variable physical properties and an arbitrary DRZ geometry. However, in addition, this work extends previous exact solutions for one-dimensional flow by: (1) allowing for a DRZ of finite but arbitrary extent, (2) accounting for depressurization due to mining the drift before drilling the borehole, and (3) accounting for two-dimensional variations of the fluid pressure caused by simultaneous fluid flow to the drift and to the borehole.

An exact solution is also presented for the ratio of the borehole fluid inflow rates determined by the two- and one-dimensional models. Sample calculations show that for some cases, two-dimensional effects dominate. In these cases the dominate flow path can be to the surface and not the borehole, even for borehole depths much greater than the borehole radius. This feature may be very important when interpreting borehole fluid collection data to determine physical properties of the DRZ.

ACKNOWLEDGMENT

The author would like to thank three people who greatly influenced this work. S. W. Webb (Department 6119) explained to the author brine inflow modeling and the significance of different aspects of the problem. D. F. McTigue (Department 1513) provided the author insight into different mechanisms for brine inflow and developed the method for calculating the brine inflow rate for the one-dimensional infinite-radius solution discussed in Section 6.0 and in Appendix B. E. J. Nowak (Department 6345) provided comments and suggestions that were very helpful to the author in writing and organizing this work.

CONTENTS

1.0	INTRODUCTION.....	1
2.0	PRESSURE PROFILE FOR THE TWO-DIMENSIONAL FINITE-RADIUS MODEL.....	11
2.1	Solution for Uniform Constant Initial Pressure in the DRZ....	21
2.2	Solution for Depth-Dependent Initial Pressure in the DRZ.....	22
3.0	PRESSURE PROFILE FOR THE TWO-DIMENSIONAL INFINITE-RADIUS MODEL....	25
3.1	Solution for Uniform Constant Initial Pressure in the DRZ....	33
3.2	Solution for Depth-Dependent Initial Pressure in the DRZ.....	35
4.0	PRESSURE PROFILE FOR THE ONE-DIMENSIONAL FINITE-RADIUS MODEL	37
5.0	PRESSURE PROFILE FOR THE ONE-DIMENSIONAL INFINITE-RADIUS MODEL ...	39
6.0	FLUID PRODUCTION INTO THE BOREHOLE AND INTO THE DRIFT.....	41
7.0	CUMULATIVE FLUID PRODUCTION.....	51
8.0	SAMPLE CALCULATIONS.....	55
8.1	Sample Calculations of Two-Dimensional Contours of the Dimensionless Pressure.....	58
8.2	Sample Calculations of Borehole Brine Inflow Rates.....	66
8.2.1	Flow Rate as $t \rightarrow 0$	66
8.2.2	Model with Maximum Flow Rate.....	74
8.2.3	Flow Rate for Same Dimensionality but Varying DRZ Outer Radius.....	74
8.2.4	Effects of Penetration Depth Relative to Radial Distance.....	74
8.2.5	Conditional Test for Using One-Dimensional Models.....	75
8.2.6	Percentage of Flow Rate to the Borehole.....	75
8.2.7	Effect of Drilling Borehole One Year After Mining Drift.....	76

9.0 CONCLUSIONS 77

10.0 REFERENCES 79

APPENDIX A: DETERMINING EIGENVALUES IN THE RADIAL DIRECTION..... A-1

APPENDIX B: EVALUATING INTEGRAL FOR AN INFINITE RADIAL DOMAIN..... B-1

Figures

1.	Schematic diagram of one-dimensional infinite-radius model.....	2
2.	Schematic diagram of one-dimensional finite-radius model.....	5
3.	Schematic diagram of two-dimensional finite-radius model.....	6
4.	Schematic diagram of two-dimensional infinite-radius model.....	8
5.	Flow rate to the borehole for two-dimensional models divided by the flow rate to the borehole for one-dimensional models, for the same DRZ outer radius, as a function of the penetration depth divided by the borehole length, for constant initial pressure in the DRZ.....	46
6.	First radial eigenvalue as a function of the DRZ inner radius a , and the DRZ outer radius b . This plot is a solution of Equation (2-20) for $i = 1$	49
7.	Dimensionless pressure contours of $(P_f - P_a)/(P_\infty - P_a)$ at a penetration depth of $D_p = 0.2$ m, for a borehole with DRZ inner and outer radii of $a = 0.05$ m and $b = 1.0$ m, respectively, and a borehole length of $L = 3.0$ m.....	61
8.	Dimensionless pressure contours of $(P_f - P_a)/(P_\infty - P_a)$ at a penetration depth of $D_p = 1.0$ m, for a borehole with DRZ inner and outer radii of $a = 0.05$ m and $b = 1.0$ m, respectively, and a borehole length of $L = 3.0$ m.....	62
9.	Dimensionless pressure contours of $(P_f - P_a)/(P_\infty - P_a)$ at a penetration depth of $D_p = 3.0$ m, for a borehole with DRZ inner and outer radii of $a = 0.05$ m and $b = 1.0$ m, respectively, and a borehole length of $L = 3.0$ m.....	63

10. Dimensionless pressure contours of $(P_f - P_a)/(P_\infty - P_a)$ at a penetration depth of $D_p = 1.0$ m, for a borehole with DRZ inner and outer radii of $a = 0.05$ and 3.0 m, respectively, and a borehole length of $L = 3.0$ m..... 64

11. Dimensionless pressure contours of $(P_f - P_a)/(P_\infty - P_a)$ at a penetration depth of $D_p = 3.0$ m, for a borehole with DRZ inner and outer radii of $a = 0.05$ m and $b = 3.0$ m, respectively, and a borehole length of $L = 3.0$ m..... 65

12. Brine inflow rates calculated for one- and two-dimensional models for a rock permeability of $k = 10^{-20} \text{ m}^2$ 67

13. Brine inflow rates calculated for one- and two-dimensional models for a rock permeability of $k = 10^{-21} \text{ m}^2$ 68

14. Brine inflow rates calculated for one- and two-dimensional models for a rock permeability of $k = 10^{-22} \text{ m}^2$ 69

15. Percentage of flow rate to borehole for the two-dimensional model. The solid, long dash, and short dash lines are for rock permeabilities of $k = 10^{-20} \text{ m}^2$, 10^{-21} m^2 , and 10^{-22} m^2 , respectively. The asymptote for long times is given by Equation (6-15), and is independent of k 70

16. Brine inflow rates calculated for one- and two-dimensional models for a rock permeability of $k = 10^{-20} \text{ m}^2$. Time period between mining the drift and drilling the borehole = $\tau = 1$ year..... 71

17. Brine inflow rates calculated for one- and two-dimensional models for a rock permeability of $k = 10^{-21} \text{ m}^2$. Time period between mining the drift and drilling the borehole = $\tau = 1$ year..... 72

18. Brine inflow rates calculated for one- and two-dimensional models for a rock permeability of $k = 10^{-22} \text{ m}^2$. Time period between mining the drift and drilling the borehole = $\tau = 1$ year..... 73

Tables

1. Comparison of Model Features.....	3
2. Sample Calculations.....	56

NOTATION

a	borehole radius which is equal to the DRZ inner radius (m)
A	arbitrary constant
b	outer radius of DRZ (m)
B	arbitrary constant
c_f	fluid compressibility (Pa^{-1})
c_r	rock compressibility (Pa^{-1})
$C(\lambda)$	one-dimensional infinite-radius coefficient ($\text{Pa}\cdot\text{m}$)
$C_j(\lambda)$	two-dimensional infinite-radius coefficient ($\text{Pa}\cdot\text{m}$)
C_i	one-dimensional finite-radius coefficient (Pa)
C_{ij}	two-dimensional finite-radius coefficient (Pa)
D_p	penetration depth = $2(\alpha t)^{1/2}$ (m)
$[D_p/L]_*$	value of D_p/L for which specified agreement is to be obtained between one- and two-dimensional models for the brine inflow rate
e	2.718281828...
f	fluid flow rate to drift (m^3/s)
\bar{f}	cumulative fluid volume to drift (m^3)
F	fluid flow rate to borehole (m^3/s)
$F_{\%}$	percentage of flow rate to borehole for two-dimensional finite-radius model
F_{1D}	fluid flow rate to borehole for a one-dimensional model (m^3/s)
F_{2D}	fluid flow rate to borehole for a two-dimensional model (m^3/s)
\bar{F}	cumulative fluid volume to borehole (m^3)
g	implicit function, the zeros of which define the radial eigenvalue
H	depth to which DRZ extends from drift for determining initial pressure profile (m)
I	symbol to represent integral of $rR(\nu, r)R(\lambda, r)$ from $r = a$ to $r \rightarrow \infty$
$I(0, \epsilon)$	integral for infinite-radius models from $\lambda = 0$ to ϵ
i	index for radial direction
j	index for vertical downward direction
J_0	zeroth-order Bessel function of the first kind
J_1	first-order Bessel function of the first kind

k	rock permeability (m^2)
l	dummy index
L	depth of borehole (m)
L_1	shallowest depth of borehole interval (m)
L_2	deepest depth of borehole interval (m)
m	index for initial pressure profile
n	order of Bessel function
p	fluid pressure minus ambient pressure between the time the drift is mined to when the borehole is drilled (Pa)
P	fluid pressure minus ambient pressure (Pa)
P_a	ambient pressure in borehole and in drift (Pa)
P_f	fluid pressure in pore space (Pa)
P_∞	fluid pressure in undisturbed rock (Pa)
P_0	initial fluid pressure minus ambient pressure just prior to drilling borehole (Pa)
Q	either J or Y
r	radial coordinate (m)
R	radial eigenfunction
R_i	i -th radial eigenfunction
t	time (s)
t_1	starting time for cumulative flow rate (s)
t_2	ending time for cumulative flow rate (s)
t_{\max}	maximum time for which one- and two-dimensional models agree to specified tolerance for brine inflow rate (s)
T	separated temporal function
u	vertical upward fluid velocity to drift (m/s)
v	radial fluid velocity to borehole (m/s)
V	pore volume in DRZ (m^3)
W	either J or Y
x	dummy variable
Y_0	zeroth-order Bessel function of the second kind
Y_1	first-order Bessel function of the second kind
z	vertical downward coordinate (m)
Z	vertical downward eigenfunction
Z_j	j -th vertical downward eigenfunction

α	diffusion coefficient (m^2/s)
β	integration variable = λa
γ	Euler's constant (0.5772156649...)
γ_m	m-th eigenvalue for initial pressure profile (m^{-1})
Δ	incremental fluid volume produced outside DRZ (m^3)
ϵ	very small value of λ used to calculate integral to determine flow rate for one-dimensional infinite-radius model (m^{-1})
η	eigenvalue for downward direction (m^{-1})
η_j	j-th eigenvalue for downward direction (m^{-1})
λ	eigenvalue for radial direction (m^{-1})
λ_i^*	approximate value of i-th eigenvalue for radial direction (m^{-1})
λ_i	i-th eigenvalue for radial direction (m^{-1})
μ	fluid viscosity ($\text{Pa}\cdot\text{s}$)
ν	dummy radial eigenvalue (m^{-1})
ξ	dummy variable of integration = $b(\lambda-\nu)$
π	3.141592654...
ρ	fluid density (kg/m^3)
ρ_a	fluid density at ambient conditions (kg/m^3)
ρ_∞	fluid density in undisturbed rock (kg/m^3)
σ	dummy index
τ	time from mining drift (s)
ϕ	porosity
ψ	dummy variable of integration = $b(\lambda+\nu)$
\ln	natural logarithm
∇^2	Laplacian operator (m^{-2})
∞	infinity
=	equal to
\neq	not equal to
\leq	less than or equal to
\geq	greater than or equal to
<	less than
>	greater than

\ll	much less than
\gg	much greater than
\rightarrow	approaches
\times	times
Σ	summation
\int	integral
\cdot	product sign for units

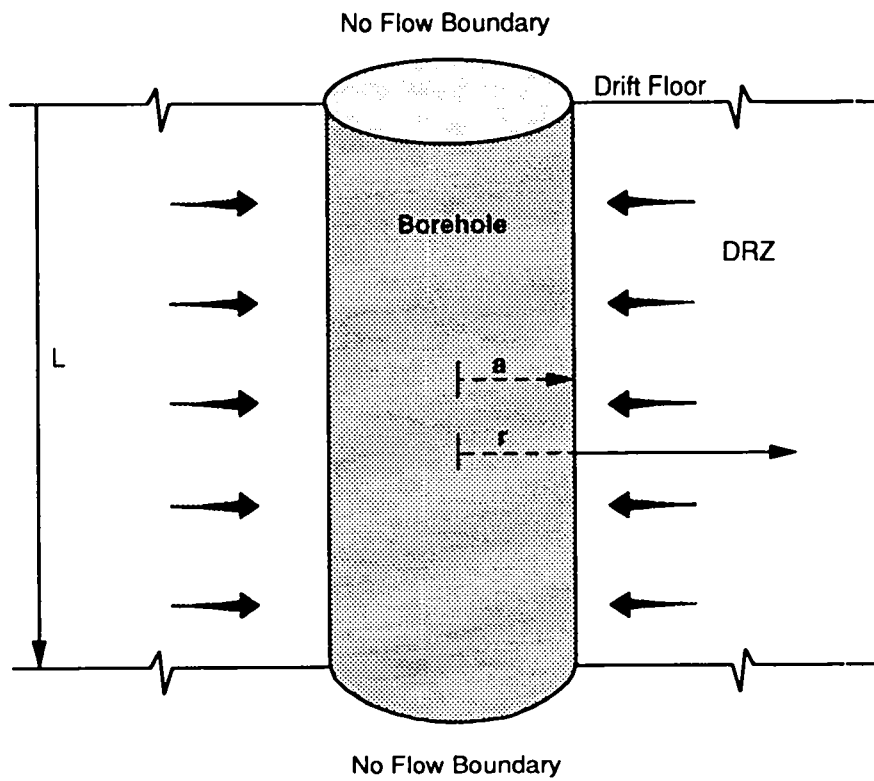
1.0 INTRODUCTION

A mathematical model is needed to estimate rock properties from data on fluid flow rates into boreholes. One model that has been used for halite at the Waste Isolation Pilot Plant (WIPP) assumes that the rock is a brine-saturated porous medium of infinite extent perpendicular to the axis of the borehole (Nowak and McTigue, 1987; Nowak et al., 1988). A schematic diagram of this model is given in Figure 1. In this one-dimensional infinite-radius model, a borehole is drilled into undisturbed rock that contains fluid under constant pressure. In the borehole, the pressure is held constant at ambient conditions, which is much lower than the fluid pressure in undisturbed rock. Brine flow into the borehole is a result of brine and rock expansion due to depressurization caused by the borehole being at this lower pressure. Darcy flow is used to model brine flow in the porous medium. A major benefit of using this model is that an exact solution is available for determining the brine flow rate into the borehole for a constant initial pressure in the region (Crank, 1975, p. 87). Furthermore, a direct method has been developed to use the exact solution for data interpretation to estimate rock properties (Nowak and McTigue, 1987; McTigue and Nowak, 1987; Nowak et al., 1988; Finley et al., 1992; Webb, 1992).

However, the one-dimensional infinite-radius model needs to be extended to remove the following four limitations:

- The permeable interconnected pore space cannot be finite and must be of infinite extent.
- The initial vertical pressure profile before drilling the borehole cannot be a function of depth.
- There is no upwards flow to the drift.
- There is no upwards flow to the borehole or drift from depths greater than the depth of the borehole.

These points are summarized in Table 1. The first limitation, assuming the medium is permeable for an infinite distance away from the borehole, conflicts with the observed apparent impermeability of halite. However, halite cannot be completely impermeable because brine inflow to boreholes is observed. These two conflicting observations can be resolved by postulating that drilling induces disruptions in the halite that result in the local formation of a permeable interconnected pore space. In this work, the localized region around the borehole that allows for flow will be called a disturbed rock zone (DRZ).



TRIF-6119-10-0

Figure 1. Schematic diagram of one-dimensional infinite-radius model.

Table 1. Comparison of Model Features

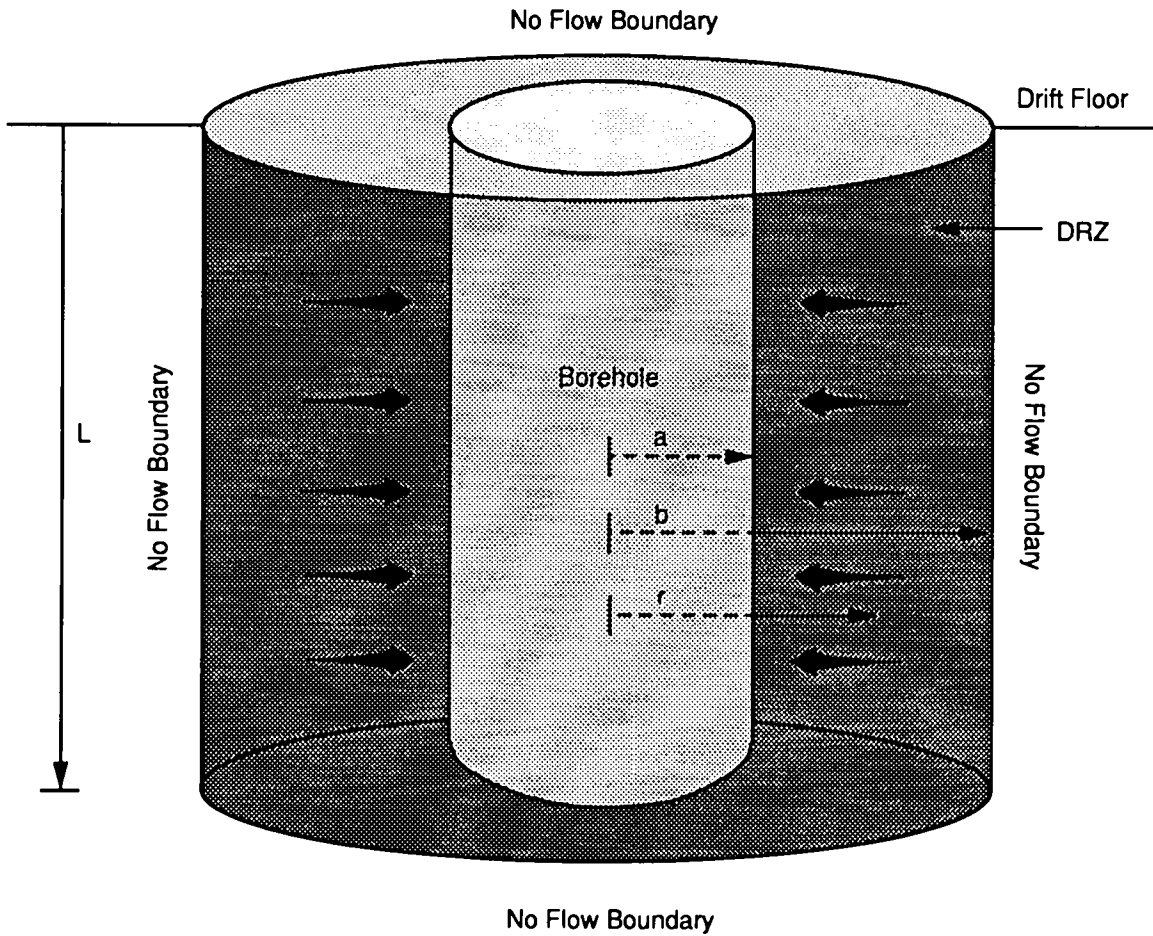
Model	Arbitrary Outer DRZ Radius	Arbitrary Initial Vertical Pressure	Vertical Flow To Drift	Vertical Flow Up From Below Borehole Depth
One-Dimensional Infinite-Radius (Figure 1)	No	No	No	No
One-Dimensional Finite-Radius (Figure 2)	Yes	No	No	No
Two-Dimensional Finite-Radius (Figure 3)	Yes	Yes	Yes	No
Two-Dimensional Infinite-Radius (Figure 4)	No	Yes	Yes	No

Beyond the DRZ, the rock is assumed to be impermeable. In contrast to the infinite-radius model, a finite-radius model (shown in Figure 2) more accurately represents the concept of a finite DRZ. The finite-radius model provides much more flexibility because it can be made to approach an infinite-radius DRZ model by assigning a very large value to the outer radius of the DRZ. Although the finite-radius model is more versatile, it introduces an additional unknown because the extent of the DRZ is not determined by the model, but must be specified independently.

The second limitation of the one-dimensional infinite-radius model is the inability to account for pressures that vary with depth prior to drilling the borehole. Because boreholes are drilled from mined drifts, there are actually two steps involved in analyzing borehole brine inflow rates. The first step of mining the drift begins the depressurization process by allowing brine to escape through the floor of the drift. This fluid loss lowers the pressure adjacent to the floor of the drift relative to that at greater depths below the drift. In the second step, the borehole is drilled into this partially depressurized region, and the initial condition for the second step is the depth-dependent pressure profile created in the region by mining the drift. In this work, the term "initial condition" refers to the state just prior to drilling the borehole. The time to drill the borehole is assumed to be negligible compared to the time between completing the borehole and measuring the brine inflow rate.

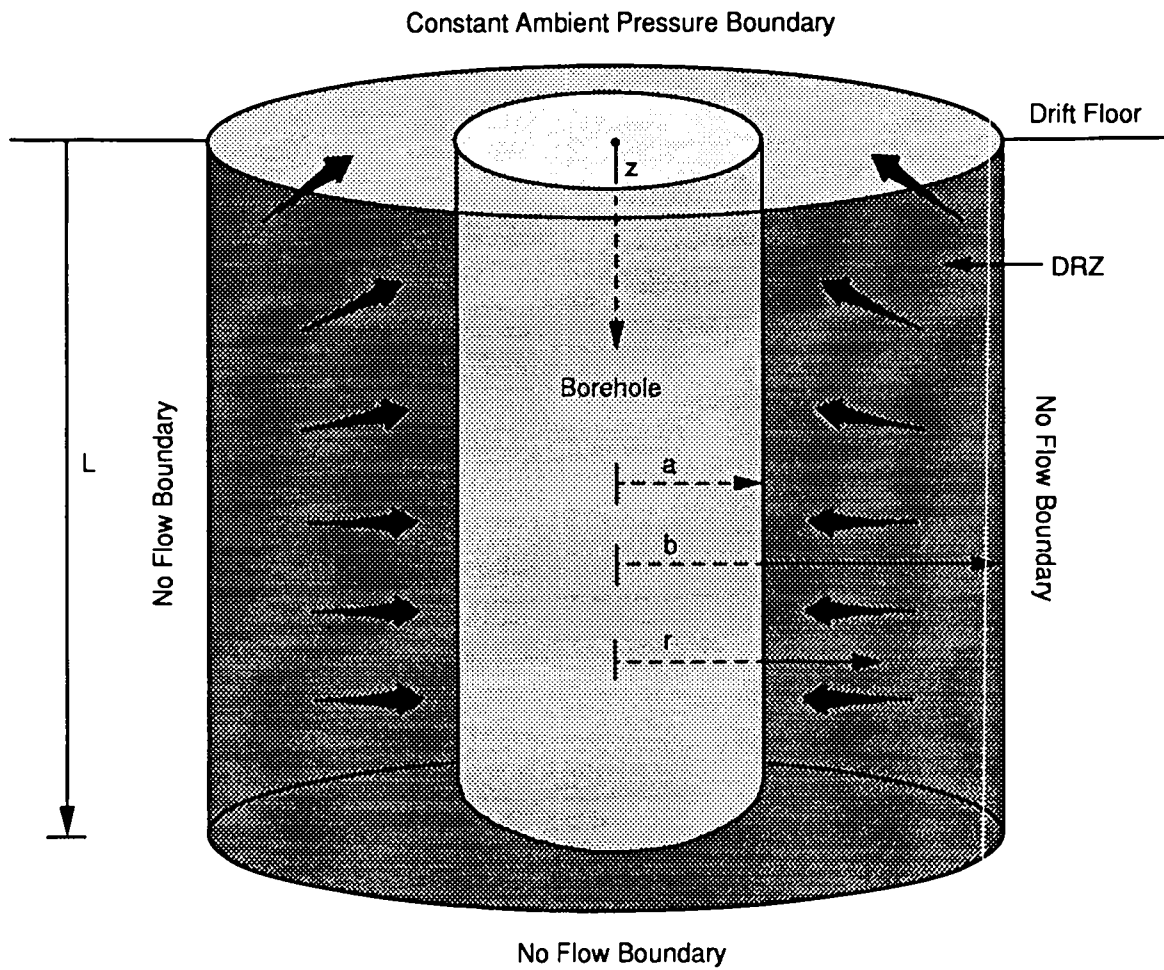
To remove the second limitation, the one-dimensional finite-radius model must be extended to a two-dimensional model, as shown in Figure 3. A two-dimensional finite-radius model can account for pressure variations with depth and radial distance from the borehole. Thus, it is possible to include a depth-dependent pressure profile formed by mining the drift. This vertical pressure profile can be used as the initial condition for determining the flow rate to a borehole. As given in Table 1, no such depth-dependent initial pressure profile can be included in either of the one-dimensional models.

The two-dimensional finite-radius model does not constrain the flow to only the borehole and thus also addresses the third limitation. Brine loss to the drift both prior to and after drilling the borehole is included in the two-dimensional model. By including the process of brine escaping into the



TRIF-6119-11-0

Figure 2. Schematic diagram of one-dimensional finite-radius model.



TRIF-6119-12-0

Figure 3. Schematic diagram of two-dimensional finite-radius model.

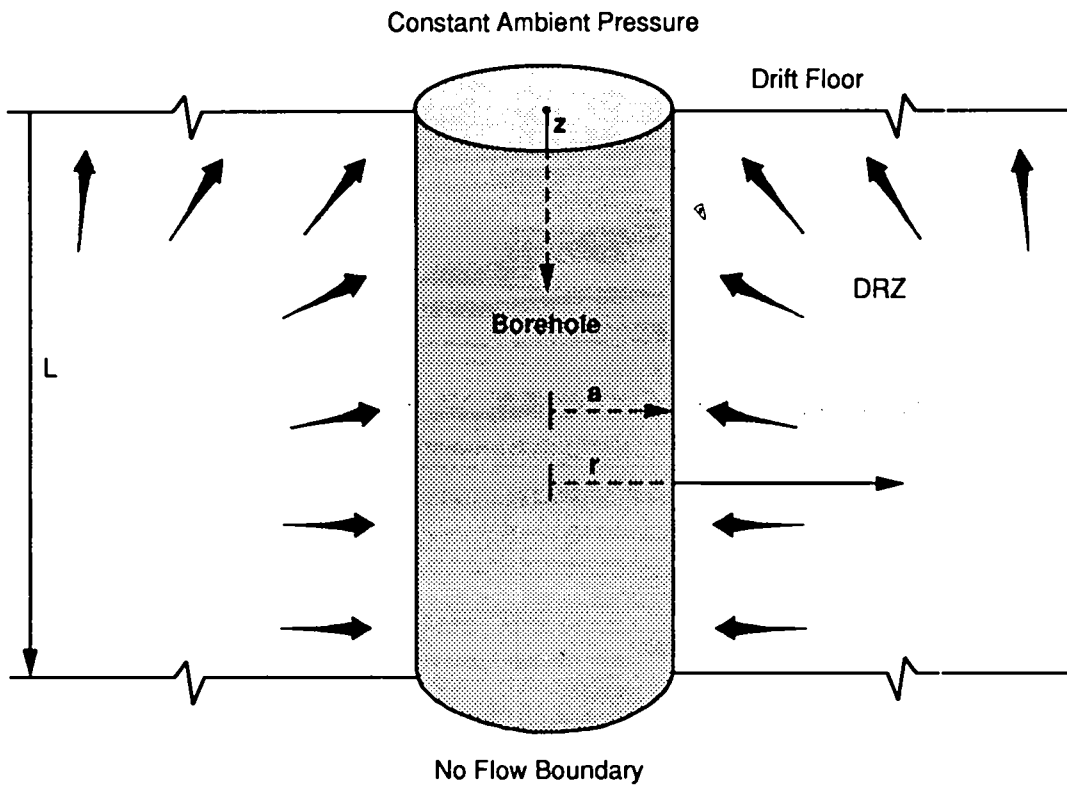
drift, the brine flow rate into the borehole is depth-dependent, even if mining the drift resulted in no significant depressurization prior to drilling the borehole. As shown in the sample calculations given in Sections 8.1 and 8.2, two-dimensional effects can be important even if the ratio of the borehole length to the borehole radius is much greater than 1. In the sample calculations, this ratio L/a , is equal to 60.

In the limit as the DRZ extends radially to infinity, the two-dimensional finite-radius model reduces to the two-dimensional infinite-radius model shown in Figure 4. As given in Table 1, because the two-dimensional infinite-radius model is restricted to a DRZ that is radially infinite, this model is less versatile than the two-dimensional finite-radius model. However, this limiting case may be appropriate if the borehole is drilled in the middle of a very large drift.

Although the two-dimensional finite-radius model derived in this work addresses the first three limitations given in Table 1, the model does not address the fourth limitation of fluid moving up from below the depth of the borehole. By this mechanism, fluid enters the borehole through the bottom surface of the borehole and through the cylindrical surface of the borehole. Further work is planned to incorporate this upward flow into the two-dimensional model.

The two-dimensional models can be used for any cylindrical hole drilled perpendicular to a flat surface, such as the floor of a drift. The surface orientation of the models is arbitrary; the models can be applied to vertical boreholes such as those in Room D at the WIPP, to horizontal boreholes such as in Room L4, and even to Room Q. However, for convenience, the models are discussed for a borehole drilled vertically down from the floor of a drift as shown in Figure 3.

The problem of two-dimensional Darcy flow caused by depressurization of a single-phase fluid in a porous medium is governed by the Diffusion Equation (Freeze and Cherry, 1979). Solutions to the Diffusion Equation for many different geometries and boundary conditions are well known (Carslaw and Jaeger, 1959; Crank, 1975). In particular, solutions applicable to problems similar to those in this work have been reported (Nicholson, 1921; Goldstein, 1932). However, no solution was found in standard texts on diffusive



TRIF-6119-13-0

Figure 4. Schematic diagram of two-dimensional infinite-radius model.

transport (Carslaw and Jaeger, 1959; Crank, 1975), for two-dimensional flow to a borehole with the initial condition of an arbitrary depth-dependent pressure in the medium.

Therefore, in Section 2.0 of this report, a detailed derivation of a two-dimensional finite-radius solution is presented for an arbitrary depth-dependent initial pressure at the time the borehole is drilled. In Section 2.1, the solution is determined explicitly for the special case of constant initial pressure in the DRZ. In Section 2.2 the solution is given for the second special case of a depth-dependent initial pressure that results from mining the drift an arbitrary amount of time before drilling the borehole. The model for the limiting case of a two-dimensional DRZ extending radially to infinity is derived in Section 3.0 for an arbitrary depth-dependent pressure profile. Solutions for the special cases of a constant initial pressure and an initial pressure resulting from mining a drift are derived in Sections 3.1 and 3.2, respectively. The solutions given in Sections 2.1 and 3.1 form the basis for deriving solutions to the one-dimensional models.

The one-dimensional finite-radius solution is developed in Section 4.0 from the two-dimensional finite-radius solution. For comparison, the limiting case of flow in a one-dimensional infinite-radius domain is given in Section 5.0. In Section 6.0, the results of Sections 2.1, 2.2, 3.1, and 3.2 are used to derive expressions for the flow rate into the borehole and to the drift for two-dimensional flow. Also in Section 6.0, the results of Sections 4.0 and 5.0 for one-dimensional flows are used to obtain expressions for the brine inflow rates for the finite-radius and the infinite-radius one-dimensional models, respectively. From the analyses for two- and one-dimensional flow, a quantitative conditional test is developed for determining when two-dimensional effects are important. This test provides a very simple but exact expression for the ratio of flow rates to the borehole for the two- and one-dimensional models. Using this test, it is shown that for the same DRZ outer radius, one-dimensional models always overestimate the brine inflow rate when compared to two-dimensional models. In Section 7.0 expressions are derived for the cumulative fluid volume produced in the borehole and into the drift. In Section 8.0, general features of the sample calculations are discussed for the range of parameters typically expected at the WIPP. Due to the large number of parameters required to model brine inflow, the concept of a penetration depth is introduced to provide a single

scaling parameter. In Sections 8.1 and 8.2, the penetration depth is shown to provide a measure of the extent to which depressurization has occurred in the DRZ. Two-dimensional contour plots of the pressure are discussed in Section 8.1. In Section 8.2 calculation results are compared for the four models given in Table 1. It is shown that in some cases, the dominant flow path can be to the drift floor and not into the borehole. The effects of mining the drift a significant amount of time before drilling the borehole are also shown in Section 8.2. Important conclusions of this work are given in Section 9.0.

2.0 PRESSURE PROFILE FOR THE TWO-DIMENSIONAL FINITE-RADIUS MODEL

The governing equation for fluid pressure minus ambient pressure in a saturated, homogeneous, isotropic porous medium with constant permeability and porosity, for a slightly compressible liquid with constant viscosity, is given by the Diffusion Equation (Freeze and Cherry, 1979)

$$\nabla^2 P = \frac{1}{\alpha} \frac{\partial P}{\partial t} \quad (2-1)$$

where

$$P = P_f - P_a \text{ (Pa)}$$

$$P_f = \text{fluid pressure in pore space (Pa)}$$

$$P_a = \text{ambient pressure adjacent to porous medium, assumed constant (Pa)}$$

$$t = \text{time (s)}$$

$$\nabla^2 = \text{Laplacian operator (m}^{-2}\text{)}$$

$$\alpha = \text{diffusion coefficient (m}^2\text{/s)}$$

The diffusion coefficient is given by (Webb, 1992, p. 13)

$$\alpha = \frac{k}{\mu [\phi c_f + c_r]} \quad (2-2)$$

where

$$k = \text{rock permeability (m}^2\text{)}$$

$$\mu = \text{fluid viscosity (Pa}\cdot\text{s)}$$

$$c_f = \text{fluid compressibility (Pa}^{-1}\text{)}$$

$$c_r = \text{rock compressibility (Pa}^{-1}\text{)}$$

$$\phi = \text{porosity.}$$

In this work, α is assumed constant, and gravitational effects are neglected. For a vertical borehole drilled from a mined horizontal surface,

the fluid pressure is a function of radial distance, depth, and time. Thus, in this case, Equation (2-1) reduces to

$$\frac{\partial^2 P}{\partial r^2} + \frac{1}{r} \frac{\partial P}{\partial r} + \frac{\partial^2 P}{\partial z^2} = \frac{1}{\alpha} \frac{\partial P}{\partial t} \quad 0 \leq z \leq L \quad \text{and} \quad a \leq r \leq b \quad (2-3)$$

where r is the radial distance measured from the axis of the borehole, and z is the vertical distance measured downward from the floor of the drift, as shown in Figure 3.

In this analysis, the size of the region that is disturbed by drilling is arbitrary but finite. Thus, to a first approximation, this region will be uniform in physical properties and will extend from the borehole out to a radius b for the entire length of the borehole, as shown in Figure 3. It is assumed that there is no fluid flow beyond this DRZ. Ambient pressure variations are assumed to be small compared to the pressure changes in the porous medium, and thus the pressure at $z = 0$, the surface of the medium, is held constant. For these conditions, the initial and boundary conditions on Equation (2-3) are given by

$$P = P_0(r, z) \quad \text{at } t = 0, \quad 0 \leq z \leq L, \quad a \leq r \leq b \quad (2-4)$$

$$P = 0 \quad \text{at } t > 0, \quad 0 \leq z \leq L, \quad r = a \quad (2-5)$$

$$\frac{\partial P}{\partial r} = 0 \quad \text{at } t > 0, \quad 0 \leq z \leq L, \quad r = b \quad (2-6)$$

$$P = 0 \quad \text{at } t > 0, \quad z = 0, \quad a \leq r \leq b \quad (2-7)$$

$$\frac{\partial P}{\partial z} = 0 \quad \text{at } t > 0, \quad z = L, \quad a \leq r \leq b \quad (2-8)$$

where L = length of the borehole (m)

a = borehole radius which is equal to DRZ inner radius (m)

b = outer radius of DRZ (m)

P_0 = fluid pressure minus the ambient pressure at time zero (Pa).

P_0 can be a function of depth because the borehole may be drilled after considerable changes in pressure occur after mining the drift. For generality, the following analysis in this section allows for P_0 to be an arbitrary function of radial distance and depth, but for the applications used in this work, P_0 will not vary with radial distance.

Equation (2-3) may be solved by the method of Separation of Variables by assuming $P(r,z,t)$ is given by

$$P(r,z,t) = R(r)Z(z)T(t) \quad (2-9)$$

where R is a function only of r , Z is a function only of z , and T is a function only of t . Substituting Equation (2-9) into Equation (2-3) and dividing by P results in

$$\frac{1}{R} \frac{d^2 R}{dr^2} + \frac{1}{rR} \frac{dR}{dr} = \frac{1}{\alpha T} \frac{dT}{dt} - \frac{1}{Z} \frac{d^2 Z}{dz^2} = -\lambda^2 \quad (2-10)$$

where $-\lambda^2$ has been chosen as the separation constant. The equation for R reduces to the zeroth-order Bessel's Equation given by (Abramowitz and Stegun, 1970, p. 358, Eq. 9.1.1; Watson, 1958)

$$\frac{d^2 R}{dr^2} + \frac{1}{r} \frac{dR}{dr} + \lambda^2 R = 0 \quad \text{for } a \leq r \leq b \quad (2-11)$$

From Equations (2-5) and (2-6), the boundary conditions on R are given by

$$R = 0 \quad \text{at } r = a \quad (2-12)$$

$$\frac{dR}{dr} = 0 \quad \text{at } r = b \quad . \quad (2-13)$$

The general solution to Equation (2-11) is given by

$$R = AJ_0(\lambda r) + BY_0(\lambda r) \quad (2-14)$$

where J_0 = zeroth-order Bessel function of the first kind
 Y_0 = zeroth-order Bessel function of the second kind
 A = constant
 B = constant.

From Equation (2-12),

$$0 = AJ_0(\lambda a) + BY_0(\lambda a) \quad . \quad (2-15)$$

Using the identities (Abramowitz and Stegun, 1970, p. 361, Eq. 9.1.28)

$$\frac{dJ_0(\lambda r)}{dr} = -\lambda J_1(\lambda r) \quad (2-16)$$

and

$$\frac{dY_0(\lambda r)}{dr} = -\lambda Y_1(\lambda r) \quad , \quad (2-17)$$

Equation (2-13) reduces to

$$0 = -A\lambda J_1(\lambda b) - B\lambda Y_1(\lambda b) \quad (2-18)$$

where J_1 and Y_1 are the first-order Bessel functions of the first and second kind, respectively.

From Equations (2-15) and (2-18), R is determined within a multiplicative constant and is given by

$$R_i = Y_0(\lambda_i a)J_0(\lambda_i r) - J_0(\lambda_i a)Y_0(\lambda_i r) \quad i = 1, 2, 3, \dots \quad (2-19)$$

where λ_i is the i -th eigenvalue given by the roots of the equation

$$0 = Y_0(\lambda_i a)J_1(\lambda_i b) - Y_1(\lambda_i b)J_0(\lambda_i a) \quad i = 1, 2, 3, \dots \quad (2-20)$$

An efficient numerical method for determining the eigenvalues λ_i is given in Appendix A.

Equation (2-10) may be separated further to give

$$\frac{1}{Z} \frac{d^2 Z}{dz^2} = \lambda_i^2 + \frac{1}{\alpha T} \frac{dT}{dt} = -\eta^2 \quad (2-21)$$

where $-\eta^2$ has been chosen as the separation constant. The equation for Z reduces to

$$\frac{d^2 Z}{dz^2} + \eta^2 Z = 0 \quad (2-22)$$

subject to the boundary conditions obtained from Equations (2-7) and (2-8). Thus, the boundary conditions on Z are given by

$$Z = 0 \quad \text{at } z = 0 \quad (2-23)$$

$$\frac{dZ}{dz} = 0 \quad \text{at } z = L \quad (2-24)$$

The solution to Equations (2-22) to (2-24) is given within a multiplicative constant by

$$Z_j = \sin[\eta_j z] \quad j = 1, 2, 3, \dots \quad (2-25)$$

where the eigenvalues η_j are given by

$$\eta_j = \frac{(2j-1)\pi}{2L} \quad j = 1, 2, 3, \dots \quad (2-26)$$

From Equation (2-21), T is governed by

$$\frac{dT}{dt} = -\alpha(\lambda_i^2 + \eta_j^2)T \quad (2-27)$$

and therefore given within a multiplicative constant by

$$T = \exp[-\alpha t(\lambda_i^2 + \eta_j^2)] \quad (2-28)$$

P may be determined by combining Equations (2-19), (2-25), and (2-28) to give

$$P = \sum_{i=1}^{\infty} \sum_{j=1}^{\infty} C_{ij} R_i(r) Z_j(z) \exp[-\alpha t(\lambda_i^2 + \eta_j^2)] \quad (2-29)$$

The constants C_{ij} are determined from Equation (2-4) at $t = 0$, which is given by

$$P_0(r, z) = \sum_{j=1}^{\infty} \sum_{i=1}^{\infty} C_{ij} R_i(r) Z_j(z) \quad (2-30)$$

The functions R_i and Z_j have the following orthogonality properties:

$$\int_a^b r R_i(r) R_\ell(r) dr = 0 \quad \text{for } i \neq \ell \quad (2-31)$$

$$\int_0^L Z_j(z) Z_\sigma(z) dz = 0 \quad \text{for } j \neq \sigma \quad (2-32)$$

With these orthogonality properties, C_{ij} may be determined by multiplying both sides of Equation (2-30) by $r R_\ell Z_\sigma$ and integrating over r from a to b , and over z from 0 to L . This results in

$$C_{ij} = \frac{\int_0^L \int_a^b r R_i(r) Z_j(z) P_0(r, z) dr dz}{\int_0^L Z_j^2(z) dz \int_a^b r R_i^2(r) dr} \quad (2-33)$$

For the applications in this work, P_0 is only a function of z , and therefore Equation (2-33) simplifies to

$$C_{ij} = \frac{\int_0^L P_0(z) Z_j(z) dz}{\int_0^L Z_j^2(z) dz} \frac{\int_a^b r R_i(r) dr}{\int_a^b r R_i^2(r) dr} . \quad (2-34)$$

Three of the integrals in Equation (2-34) are independent of P_0 and thus can be determined regardless of the initial depth-dependent pressure profile.

The square of the norm of Z_j is given by

$$\int_0^L Z_j^2(z) dz = \frac{L}{2} . \quad (2-35)$$

Using the identities (Abramowitz and Stegun, 1970, p. 361, Eq. 9.1.30)

$$\int x J_0(x) dx = x J_1(x) \quad (2-36)$$

$$\int x Y_0(x) dx = x Y_1(x) , \quad (2-37)$$

the first moment of R_i is given by

$$\int_a^b rR_i(r) dr = \frac{b}{\lambda_i} \left[Y_0(\lambda_i a)J_1(\lambda_i b) - J_0(\lambda_i a)Y_1(\lambda_i b) \right] \\ - \frac{a}{\lambda_i} \left[Y_0(\lambda_i a)J_1(\lambda_i a) - J_0(\lambda_i a)Y_1(\lambda_i a) \right] . \quad (2-38)$$

The first term in square brackets on the right-hand-side of Equation (2-38) is zero from Equation (2-20). Therefore,

$$\int_a^b rR_i(r) dr = - \frac{a}{\lambda_i} \left[Y_0(\lambda_i a)J_1(\lambda_i a) - J_0(\lambda_i a)Y_1(\lambda_i a) \right] . \quad (2-39)$$

Because the Wronskian of the Bessel functions is given by (Abramowitz and Stegun, 1970, p. 360, Eq. 9.1.16)

$$Y_0(x)J_1(x) - J_0(x)Y_1(x) = \frac{2}{\pi x} , \quad (2-40)$$

Equation (2-39) reduces to

$$\int_a^b rR_i(r) dr = - \frac{2}{\pi \lambda_i^2} . \quad (2-41)$$

Using an identity for the integral of a product of Bessel functions (Abramowitz and Stegun, 1970, p. 484, Eq. 11.3.31),

$$\int xW_0(x)Q_0(x) dx = \frac{x^2}{2} \left[Q_0(x)W_0(x) + Q_1(x)W_1(x) \right] \quad \begin{matrix} (Q = J \text{ or } Y) \\ (W = J \text{ or } Y) \end{matrix} , \quad (2-42)$$

we have that

$$\int_a^b rR_i^2(r) dr = \frac{b^2}{2} \left[[Y_0(\lambda_i a)J_0(\lambda_i b) - J_0(\lambda_i a)Y_0(\lambda_i b)]^2 + [Y_0(\lambda_i a)J_1(\lambda_i b) - J_0(\lambda_i a)Y_1(\lambda_i b)]^2 \right] - \frac{a^2}{2} \left[Y_0(\lambda_i a)J_1(\lambda_i a) - J_0(\lambda_i a)Y_1(\lambda_i a) \right]^2 . \quad (2-43)$$

Using Equation (2-20) to eliminate the second cross product of Bessel functions in Equation (2-43) and Equation (2-40) for the third cross product, we have that

$$\int_a^b rR_i^2(r) dr = \frac{b^2}{2} \left[Y_0(\lambda_i a)J_0(\lambda_i b) - J_0(\lambda_i a)Y_0(\lambda_i b) \right]^2 - \frac{2}{\pi^2 \lambda_i^2} . \quad (2-44)$$

Equation (2-44) may be further simplified by solving Equation (2-20) for $Y_0(\lambda_i a)$, substituting it into Equation (2-44) and reapplying Equation (2-40) to give

$$\int_a^b rR_i^2 dr = \frac{2}{\pi^2 \lambda_i^2} \left[\frac{J_0^2(\lambda_i a)}{J_1^2(\lambda_i b)} - 1 \right] . \quad (2-45)$$

Combining Equations (2-34), (2-35), (2-41), and (2-45) results in

$$C_{ij} = \frac{2\pi}{L} \left[\frac{J_1^2(\lambda_i b)}{J_1^2(\lambda_i b) - J_0^2(\lambda_i a)} \right] \int_0^L P_0(z) Z_j(z) dz \quad (2-46)$$

The pressure at any point in the domain at any time can be calculated using Equations (2-29) and (2-46). This solution is for an arbitrary initial fluid pressure that varies with depth. For this work, there are two initial fluid pressures of interest. In the first case, the borehole is drilled very soon after mining the drift such that P_0 is essentially a constant throughout the DRZ. In the second case, there is a considerable time period from when the drift is mined until the borehole is drilled. In this second case, the initial fluid pressure is more complicated, but the integral given in Equation (2-46) can still be evaluated analytically. The solutions for both cases are presented below in Sections 2.1 and 2.2, respectively.

2.1 Solution for Uniform Constant Initial Pressure in the DRZ

For P_0 equal to a constant, $P_\infty - P_a$, where P_∞ is the pressure in undisturbed rock, Equation (2-46) reduces to

$$C_{ij} = \frac{4(P_\infty - P_a)}{(2j - 1)} \left[\frac{J_1^2(\lambda_i b)}{J_1^2(\lambda_i b) - J_0^2(\lambda_i a)} \right] \quad (2-47)$$

Substituting Equations (2-19), (2-25), and (2-47) into Equation (2-29) results in the solution for uniform initial pressure, which is given by

$$P = \sum_{i=1}^{\infty} \sum_{j=1}^{\infty} \frac{4(P_{\infty} - P_a) J_1^2(\lambda_i b) \sin[\eta_j z] \{Y_0(\lambda_i a) J_0(\lambda_i r) - J_0(\lambda_i a) Y_0(\lambda_i r)\}}{(2j-1) [J_1^2(\lambda_i b) - J_0^2(\lambda_i a)]} \times \exp[-\alpha t (\lambda_i^2 + \eta_j^2)] \quad (2-48)$$

where λ_i is given by Equation (2-20), and η_j is given by Equation (2-26).

The expression given in Equation (2-48) may be factored into two parts, one completely determined by the index i , and the other completely determined by the index j . Thus, instead of evaluating a double summation, it is computationally faster to evaluate Equation (2-48) as a product of two summations, one on i and the other on j . By performing this factorization, Equation (2-48) can be evaluated as

$$P = \left[\sum_{i=1}^{\infty} \frac{4(P_{\infty} - P_a) J_1^2(\lambda_i b) [Y_0(\lambda_i a) J_0(\lambda_i r) - J_0(\lambda_i a) Y_0(\lambda_i r)] \exp[-\alpha t \lambda_i^2]}{J_1^2(\lambda_i b) - J_0^2(\lambda_i a)} \right] \times \left[\sum_{j=1}^{\infty} \frac{[\sin[\eta_j z]] \exp[-\alpha t \eta_j^2]}{2j - 1} \right] \quad (2-49)$$

2.2 Solution for Depth-Dependent Initial Pressure in the DRZ

For a mined horizontal surface, the fluid pressure adjacent to the surface is assumed to vary only with depth and time. In this case Equation (2-1) reduces to the classical one-dimensional Diffusion Equation given by

$$\frac{\partial^2 p}{\partial z^2} = \frac{1}{\alpha} \frac{\partial p}{\partial \tau} \quad 0 \leq z \leq H \quad (2-50)$$

where p is the fluid pressure minus the ambient pressure, τ is the time from when the floor of the drift is mined and is not equal to t , the time from when the borehole is drilled. In the process of mining a drift, the rock is assumed to be altered to allow fluid flow up to an arbitrary but finite depth H . At depths greater than H , no flow is assumed. The value of H is not determined in this work and must be specified independently. Because the depth of the DRZ may be only several meters, the fluid pressure just prior to mining the drift is assumed independent of depth and is taken as a constant $P_\infty - P_a$ for $0 \leq z \leq H$.

With these modeling assumptions, the conditions on Equation (2-50) are given by

$$p = P_\infty - P_a \quad \text{at } \tau = 0, 0 \leq z \leq H \quad (2-51)$$

$$p = 0 \quad \text{at } \tau > 0, z = 0 \quad (2-52)$$

$$\frac{\partial p}{\partial z} = 0 \quad \text{at } \tau > 0, z = H \quad (2-53)$$

The solution to Equations (2-50) to (2-53) may be obtained by the method of Separation of Variables, and is given by

$$p = \sum_{m=1}^{\infty} \left[\frac{4(P_\infty - P_a)}{(2m-1)\pi} \right] \sin[\gamma_m z] \exp[-\alpha \tau \gamma_m^2] \quad (2-54)$$

where the eigenvalues are given by

$$\gamma_m = \frac{(2m-1)\pi}{2H} \quad (2-55)$$

From Equation (2-54), $p/(P_\infty - P_a)$ is a function only of two dimensionless groups, a dimensionless distance z/H , and a dimensionless time $\alpha \tau / H^2$. For

long times as $\alpha\tau/H^2 \rightarrow \infty$, the fluid drains to the surface $z = 0$ until the pressure throughout the DRZ goes to the ambient pressure.

If the borehole is drilled at time τ , then $P_0(z) = p(z, \tau)$, and substituting Equation (2-54) into Equation (2-46) results in

$$C_{ij} = \begin{cases} \frac{\pi}{L} \left[\frac{2J_1^2(\lambda_i b)(P_\infty - P_a)}{J_1^2(\lambda_i b) - J_0^2(\lambda_i a)} \right] \left[\frac{\cos(\eta_j H)}{\eta_j} + \sum_{m=1}^{\infty} \frac{4\theta_{jm}(H)}{(2m-1)\pi} \exp(-\alpha\tau\gamma_m^2) \right] & \text{for } H < L \\ \left[\frac{J_1^2(\lambda_i b)(P_\infty - P_a)}{J_1^2(\lambda_i b) - J_0^2(\lambda_i a)} \right] \left[\frac{4}{(2j-1)} \exp(-\alpha\tau\eta_j^2) \right] & \text{for } H = L \\ \frac{\pi}{L} \left[\frac{2J_1^2(\lambda_i b)(P_\infty - P_a)}{J_1^2(\lambda_i b) - J_0^2(\lambda_i a)} \right] \left[\sum_{m=1}^{\infty} \frac{4\theta_{jm}(L)}{(2m-1)\pi} \exp(-\alpha\tau\gamma_m^2) \right] & \text{for } H > L \end{cases} \quad (2-56)$$

where $\theta_{jm}(x)$ is given by

$$\theta_{jm}(x) = \begin{cases} \frac{\sin[x(\eta_j - \gamma_m)]}{2(\eta_j - \gamma_m)} - \frac{\sin[x(\eta_j + \gamma_m)]}{2(\eta_j + \gamma_m)} & \text{for } \eta_j \neq \gamma_m \\ \frac{x}{2} - \frac{\sin(2\eta_j x)}{4\eta_j} & \text{for } \eta_j = \gamma_m \end{cases} \quad (2-57)$$

The complete solution for this case is given by Equation (2-29) with C_{ij} determined from Equation (2-56) with τ equal to the time between mining the drift and drilling the borehole.

3.0 PRESSURE PROFILE FOR THE TWO-DIMENSIONAL INFINITE-RADIUS MODEL

The governing equation for a two-dimensional infinite-radius model is the same as that given by Equation (2-3), except that as shown in Figure 4, the domain of the problem is over the region $a \leq r < \infty$. Therefore, the equation and boundary conditions to be solved are given by

$$\frac{\partial^2 P}{\partial r^2} + \frac{1}{r} \frac{\partial P}{\partial r} + \frac{\partial^2 P}{\partial z^2} = \frac{1}{\alpha} \frac{\partial P}{\partial t} \quad 0 \leq z \leq L \quad \text{and} \quad a \leq r < \infty \quad (3-1)$$

$$P = P_0(z) \quad \text{at } t = 0, \quad 0 \leq z \leq L, \quad a \leq r < \infty \quad (3-2)$$

$$P = 0 \quad \text{at } t > 0, \quad 0 \leq z \leq L, \quad r = a \quad (3-3)$$

$$P \rightarrow P(z, t) \quad \text{at } t > 0, \quad 0 \leq z \leq L, \quad r \rightarrow \infty \quad (3-4)$$

$$P = 0 \quad \text{at } t > 0, \quad z = 0, \quad a \leq r < \infty \quad (3-5)$$

$$\frac{\partial P}{\partial z} = 0 \quad \text{at } t > 0, \quad z = L, \quad a \leq r < \infty \quad (3-6)$$

Equation (3-4) states that as $r \rightarrow \infty$, P is independent of r . This condition therefore requires that as $r \rightarrow \infty$, the partial derivative of P with respect to r is zero.

The system given by Equations (3-1) to (3-6) is solved by the method of Separation of Variables, using the same notation as in Equation (2-9). The vertical eigenfunction $Z(z)$ is the same as that for the two-dimensional finite-radius model given by Equations (2-25) and (2-26). The radial eigenfunction $R(\lambda, r)$ is governed by

$$\frac{d^2 R}{dr^2} + \frac{1}{r} \frac{dR}{dr} + \lambda^2 R = 0 \quad \text{for } a \leq r < \infty \quad (3-7)$$

From Equations (3-3) and (3-4), the boundary conditions on R are given by

$$R = 0 \quad \text{at } r = a \quad (3-8)$$

$$R = \text{constant} \quad \text{as } r \rightarrow \infty \quad (3-9)$$

The general solution to Equation (3-7) is given by

$$R(\lambda, r) = AJ_0(\lambda r) + BY_0(\lambda r) \quad (3-10)$$

Equation (3-8) can be used to determine the constant A, and thus to within a multiplicative constant, $R(\lambda, r)$ is given by

$$R(\lambda, r) = Y_0(\lambda a)J_0(\lambda r) - J_0(\lambda a)Y_0(\lambda r) \quad \text{for } a \leq r < \infty \quad (3-11)$$

Equation (3-9) is automatically satisfied for $\lambda > 0$, because both $J_0(\lambda r)$ and $Y_0(\lambda r)$ approach zero as $r \rightarrow \infty$. Therefore, instead of discrete eigenvalues, $R(\lambda, r)$ will satisfy Equation (3-7) for all values of λ between 0 and ∞ . In addition, from Equations (2-16), (2-17), (3-9), and (3-11),

$$\left. \frac{dR(\lambda, r)}{dr} \right|_{r \rightarrow \infty} = -\lambda [Y_0(\lambda a)J_1(\lambda r) - J_0(\lambda a)Y_1(\lambda r)] \Big|_{r \rightarrow \infty} = 0 \quad (3-12)$$

The governing equation for T is similar to Equation (2-27), and is given by

$$\frac{dT}{dt} = -\alpha(\lambda^2 + \eta_j^2)T \quad (3-13)$$

The solution to Equation (3-13) is given within a multiplicative constant by

$$T = \exp[-\alpha t(\lambda^2 + \eta_j^2)] \quad (3-14)$$

P may be determined by combining Equations (3-11), (2-25), and (3-14) to give

$$P(r, z, t) = \sum_{j=1}^{\infty} \int_0^{\infty} C_j(\lambda) R(\lambda, r) Z_j(z) \exp\left[-\alpha t(\lambda^2 + \eta_j^2)\right] d\lambda \quad (3-15)$$

where $C_j(\lambda)$ are constants that are determined from the initial condition given by Equation (3-2).

The solution given by Equation (3-15) for a two-dimensional infinite-radius model is the limit of the solution given by Equation (2-29) as the outer limit of the DRZ extends to infinity. The primary difference is that for the infinite-radius model, in the limit as $b \rightarrow \infty$, the summation over discrete radial eigenvalues becomes an integral over continuous radial eigenvalues.

The method for extracting $C_j(\lambda)$ from Equation (3-15) at $t = 0$ is similar to that used in Section 2.0. However, there are several subtle steps because the domain is infinite. For the infinite-radius model, start with a radial domain from $r = a$ to $r = b$, and then take the limit as $b \rightarrow \infty$. This is similar to the method used to obtain the Fourier Integral over an infinite domain (Arpaci, 1966; Hildebrand, 1962; Gray et al., 1952).

At $t = 0$, Equation (3-15) reduces to

$$P_0(z) = \sum_{j=1}^{\infty} \int_0^{\infty} C_j(\lambda) R(\lambda, r) Z_j(z) d\lambda \quad (3-16)$$

Multiplying both sides of Equation (3-16) by $rR(\nu, r)Z_\nu(z)$, integrating over r from a to b , and over z from 0 to L , interchanging the order of integration and summation, and using Equation (2-32) results in

$$\int_0^L Z_j(z) P_0(z) dz \int_a^b rR(v, r) dr - \int_0^L Z_j^2(z) dz \int_0^\infty C_j(\lambda) \int_a^b rR(v, r)R(\lambda, r) dr d\lambda \quad (3-17)$$

where v is a dummy radial eigenvalue. The first integral on the right-hand side of Equation (3-17) has already been determined by Equation (2-35) and is equal to $L/2$. The second integral on the left-hand side of Equation (3-17) is similar to that given by Equation (2-38), but for a continuous eigenvalue v ,

$$\int_a^b rR(v, r) dr = \frac{b}{v} \left[Y_0(va)J_1(vb) - J_0(va)Y_1(vb) \right] - \frac{a}{v} \left[Y_0(va)J_1(va) - J_0(va)Y_1(va) \right] \quad (3-18)$$

As given by Equation (3-12), the first term in brackets on the right-hand side of Equation (3-18) goes to zero as b goes to infinity. By using Equation (2-40), Equation (3-18) reduces to

$$\int_a^b rR(v, r) dr = - \frac{2}{\pi v^2} \quad (3-19)$$

Continuing with simplifying Equation (3-17), let

$$I = \int_a^b rR(v, r)R(\lambda, r) dr \quad (3-20)$$

Substituting Equation (3-11) into Equation (3-20) and using the identity (Abramowitz and Stegun, 1970, p. 484, Eq. 11.3.29)

$$(v^2 - \lambda^2) \int r Q_0(vr) W_0(\lambda r) dr = r \left[v Q_1(vr) W_0(\lambda r) - \lambda Q_0(vr) W_1(\lambda r) \right] \quad (3-21)$$

where $Q = J$ or Y , and $W = J$ or Y , results in

$$\begin{aligned} \frac{I(v^2 - \lambda^2)}{b} &= Y_0(va) Y_0(\lambda a) \left[v J_1(vb) J_0(\lambda b) - \lambda J_0(vb) J_1(\lambda b) \right] \\ &+ J_0(va) J_0(\lambda a) \left[v Y_1(vb) Y_0(\lambda b) - \lambda Y_0(vb) Y_1(\lambda b) \right] \\ &- Y_0(va) J_0(\lambda a) \left[v J_1(vb) Y_0(\lambda b) - \lambda J_0(vb) Y_1(\lambda b) \right] \\ &- J_0(va) Y_0(\lambda a) \left[v Y_1(vb) J_0(\lambda b) - \lambda Y_0(vb) J_1(\lambda b) \right] . \end{aligned} \quad (3-22)$$

Using the trigonometric identities (Abramowitz and Stegun, 1970, p. 72)

$$\sin \left[x - \frac{\pi}{2} \right] = -\cos(x) \quad (3-23)$$

$$\cos \left[x - \frac{\pi}{2} \right] = \sin(x), \quad (3-24)$$

the asymptotic expansions (Abramowitz and Stegun, 1970, p. 364, Eqs. 9.2.1 and 9.2.2)

$$J_0(\lambda b) \rightarrow \sqrt{\frac{2}{\pi \lambda b}} \cos \left[\lambda b - \frac{\pi}{4} \right] \quad \lambda b \rightarrow \infty \quad (3-25)$$

$$J_1(\lambda b) \rightarrow \sqrt{\frac{2}{\pi \lambda b}} \sin\left[\lambda b - \frac{\pi}{4}\right] \quad \lambda b \rightarrow \infty \quad (3-26)$$

$$Y_0(\lambda b) \rightarrow \sqrt{\frac{2}{\pi \lambda b}} \sin\left[\lambda b - \frac{\pi}{4}\right] \quad \lambda b \rightarrow \infty \quad (3-27)$$

$$Y_1(\lambda b) \rightarrow -\sqrt{\frac{2}{\pi \lambda b}} \cos\left[\lambda b - \frac{\pi}{4}\right] \quad \lambda b \rightarrow \infty \quad (3-28)$$

can be obtained and used to reduce Equation (3-22) for ub and λb approaching infinity to

$$\begin{aligned} & \frac{(v^2 - \lambda^2)\pi I}{2} = \\ & Y_0(va)Y_0(\lambda a) \left(\sqrt{\frac{v}{\lambda}} \sin\left[ub - \frac{\pi}{4}\right] \cos\left[\lambda b - \frac{\pi}{4}\right] - \sqrt{\frac{\lambda}{v}} \cos\left[ub - \frac{\pi}{4}\right] \sin\left[\lambda b - \frac{\pi}{4}\right] \right) \\ & - J_0(va)J_0(\lambda a) \left(\sqrt{\frac{v}{\lambda}} \cos\left[ub - \frac{\pi}{4}\right] \sin\left[\lambda b - \frac{\pi}{4}\right] - \sqrt{\frac{\lambda}{v}} \sin\left[ub - \frac{\pi}{4}\right] \cos\left[\lambda b - \frac{\pi}{4}\right] \right) \\ & - Y_0(va)J_0(\lambda a) \left(\sqrt{\frac{v}{\lambda}} \sin\left[ub - \frac{\pi}{4}\right] \sin\left[\lambda b - \frac{\pi}{4}\right] + \sqrt{\frac{\lambda}{v}} \cos\left[ub - \frac{\pi}{4}\right] \cos\left[\lambda b - \frac{\pi}{4}\right] \right) \\ & + J_0(va)Y_0(\lambda a) \left(\sqrt{\frac{v}{\lambda}} \cos\left[ub - \frac{\pi}{4}\right] \cos\left[\lambda b - \frac{\pi}{4}\right] + \sqrt{\frac{\lambda}{v}} \sin\left[ub - \frac{\pi}{4}\right] \sin\left[\lambda b - \frac{\pi}{4}\right] \right) . \end{aligned} \quad (3-29)$$

Using Equations (3-23) and (3-24) and the identities (Abramowitz and Stegun, 1970, p. 72, Eqs. 4.3.31 to 4.3.33)

$$2\cos(x_1)\sin(x_2) = \sin(x_1 + x_2) - \sin(x_1 - x_2) \quad (3-30)$$

$$2\sin(x_1)\sin(x_2) = \cos(x_1 - x_2) - \cos(x_1 + x_2) \quad (3-31)$$

$$2\cos(x_1)\cos(x_2) = \cos(x_1 - x_2) + \cos(x_1 + x_2) , \quad (3-32)$$

Equation (3-29) reduces to

$$\begin{aligned}
I = & - \frac{Y_0(va)Y_0(\lambda a)}{\pi(v^2 - \lambda^2)} \left[\sqrt{\frac{v}{\lambda}} \sin[b(\lambda - v)] + \sqrt{\frac{\lambda}{v}} \sin[b(\lambda - v)] \right] \\
& - \frac{J_0(va)J_0(\lambda a)}{\pi(v^2 - \lambda^2)} \left[\sqrt{\frac{v}{\lambda}} \sin[b(\lambda - v)] + \sqrt{\frac{\lambda}{v}} \sin[b(\lambda - v)] \right] \\
& - \frac{Y_0(va)J_0(\lambda a)}{\pi(v^2 - \lambda^2)} \left[\sqrt{\frac{v}{\lambda}} \cos[b(\lambda - v)] + \sqrt{\frac{\lambda}{v}} \cos[b(\lambda - v)] \right] \\
& + \frac{J_0(va)Y_0(\lambda a)}{\pi(v^2 - \lambda^2)} \left[\sqrt{\frac{v}{\lambda}} \cos[b(\lambda - v)] + \sqrt{\frac{\lambda}{v}} \cos[b(\lambda - v)] \right] \\
& + \text{Terms containing } \cos[b(\lambda+v)] \text{ or } \sin[b(\lambda+v)] \quad .
\end{aligned} \tag{3-33}$$

Substituting Equations (2-35), (3-19), and (3-20) into Equation (3-17) results in

$$- \frac{4}{\pi L v^2} \int_0^L Z_j(z) P_0(z) dz = \lim_{b \rightarrow \infty} \int_0^\infty C_j(\lambda) \int_a^b I dr d\lambda \tag{3-34}$$

where I is given by Equation (3-33). Notice that I is composed of terms containing either $\cos[b(\lambda-v)]$ and $\sin[b(\lambda-v)]$, or $\cos[b(\lambda+v)]$ and $\sin[b(\lambda+v)]$. The trigonometric terms with a difference of eigenvalues are given explicitly in Equation (3-33). For these terms let

$$\xi = b(\lambda - v) \quad , \tag{3-35}$$

and for trigonometric terms with a sum of eigenvalues let

$$\psi = b(\lambda + \nu) \quad . \quad (3-36)$$

With these changes in variables, for fixed values of ξ and ψ , as $b \rightarrow \infty$, λ approaches respectively,

$$\lambda = \frac{\xi}{b} + \nu \rightarrow \nu \quad \text{as } b \rightarrow \infty \quad (3-37)$$

$$\lambda = \frac{\psi}{b} - \nu \rightarrow -\nu \quad \text{as } b \rightarrow \infty \quad . \quad (3-38)$$

Substituting Equations (3-35) and (3-36) into Equation (3-33), taking the limit of Equation (3-33) as $b \rightarrow \infty$, and using Equations (3-37) and (3-38) on the expressions $Y_0(\lambda a)$, $J_0(\lambda a)$, $(\nu/\lambda)_{1/2}$, and $(\lambda/\nu)_{1/2}$, reduces Equation (3-34) to

$$\begin{aligned} -\frac{4}{\pi L \nu^2} \int_0^L Z_j(z) P_0(z) dz &= \lim_{b \rightarrow \infty} \int_{-b\nu}^{\infty} C_j \left[\frac{\xi}{b} + \nu \right] \left[-\frac{2Y_0^2(\nu a) \sin(\xi)}{\pi \left[-\frac{2\nu\xi}{b} - \frac{\xi^2}{b^2} \right]} \right] \frac{d\xi}{b} \\ &+ \lim_{b \rightarrow \infty} \int_{-b\nu}^{\infty} C_j \left[\frac{\xi}{b} + \nu \right] \left[-\frac{2J_0^2(\nu a) \sin(\xi)}{\pi \left[-\frac{2\nu\xi}{b} - \frac{\xi^2}{b^2} \right]} \right] \frac{d\xi}{b} \quad (3-39) \\ &+ \lim_{b \rightarrow \infty} \int_{b\nu}^{\infty} C_j \left[\frac{\psi}{b} - \nu \right] [\text{trigonometric terms of } (\psi)] \frac{d\psi}{b} \end{aligned}$$

where the third and fourth terms on the right-hand side of Equation (3-33) cancel in the limit as $b \rightarrow \infty$. Also, as $b \rightarrow \infty$, the lower limit of integration approaches the upper limit of integration for the last term on the right-hand side of Equation (3-39). Therefore, this term is zero, and Equation (3-39) reduces to

$$-\frac{4}{\pi L v^2} \int_0^L Z_j(z) P_0(z) dz = \frac{C_j(v) [Y_0^2(va) + J_0^2(va)]}{\pi v} \int_{-\infty}^{\infty} \frac{\sin(\xi)}{\xi} d\xi \quad (3-40)$$

The integral on the right-hand side of Equation (3-40) is equal to π (Abramowitz and Stegun, 1970, p. 78, Eq. 4.3.142). Therefore, replacing v with λ in Equation (3-40) results in

$$C_j(\lambda) = -\frac{4}{\pi L \lambda [Y_0^2(\lambda a) + J_0^2(\lambda a)]} \int_0^L Z_j(z) P_0(z) dz \quad (3-41)$$

The pressure at any point in the domain and at any time can be calculated using Equations (3-15) and (3-41) for an arbitrary initial pressure profile given by $P_0(z)$. Two cases for P_0 are of interest and are presented in Sections 3.1 and 3.2, for P_0 constant and P_0 determined for the case of significant depressurization caused by mining the drift, respectively.

3.1 Solution for Uniform Constant Initial Pressure in the DRZ

For P_0 equal to a constant, $P_\infty - P_a$, Equation (3-41) reduces to

$$C_j(\lambda) = - \frac{8(P_\infty - P_a)}{\pi^2 \lambda (2j-1) [Y_0^2(\lambda a) + J_0^2(\lambda a)]} \quad (3-42)$$

Substituting Equations (2-25), (3-11), and (3-42) into Equation (3-15) results in the solution for the two-dimensional infinite-radius model for uniform initial pressure, which is given by

$$P = - \sum_{j=1}^{\infty} \int_0^{\infty} \frac{8(P_\infty - P_a) [Y_0(\lambda a) J_0(\lambda r) - J_0(\lambda a) Y_0(\lambda r)] \sin(\eta_j z)}{\pi^2 \lambda (2j-1) [Y_0^2(\lambda a) + J_0^2(\lambda a)]} \times \exp[-\alpha t (\lambda^2 + \eta_j^2)] d\lambda \quad (3-43)$$

For computational efficiency, Equation (3-43) may be factored into

$$P = \left(- \int_0^{\infty} \frac{8(P_\infty - P_a) [Y_0(\lambda a) J_0(\lambda r) - J_0(\lambda a) Y_0(\lambda r)] \exp(-\alpha t \lambda^2)}{\pi^2 \lambda [Y_0^2(\lambda a) + J_0^2(\lambda a)]} d\lambda \right) \times \left(\sum_{j=1}^{\infty} \frac{[\sin(\eta_j z)] \exp[-\alpha t \eta_j^2]}{2j - 1} \right) \quad (3-44)$$

Equation (3-44) eliminates the need to evaluate repeatedly the integral in Equation (3-43).

3.2 Solution for Depth-Dependent Initial Pressure in the DRZ

For $P_0(z)$ given by Equation (2-54), the integral in Equation (3-41) may be evaluated to give

$$C_j(\lambda) = \begin{cases} \frac{4}{\pi L \lambda} \left[\frac{P_a - P_\infty}{Y_0^2(\lambda a) - J_0^2(\lambda a)} \right] \left[\frac{\cos(\eta_j H)}{\eta_j} + \sum_{m=1}^{\infty} \frac{4\theta_{jm}(H)}{(2m-1)\pi} \exp\{-\alpha r \gamma_m^2\} \right] & \text{for } H < L \\ \frac{2}{\pi^2 \lambda} \left[\frac{P_a - P_\infty}{Y_0^2(\lambda a) - J_0^2(\lambda a)} \right] \left[\frac{4}{(2j-1)} \exp\{-\alpha r \eta_j^2\} \right] & \text{for } H = L \\ \frac{4}{\pi L \lambda} \left[\frac{P_a - P_\infty}{Y_0^2(\lambda a) - J_0^2(\lambda a)} \right] \left[\sum_{m=1}^{\infty} \frac{4\theta_{jm}(L)}{(2m-1)\pi} \exp\{-\alpha r \gamma_m^2\} \right] & \text{for } H > L \end{cases} \quad (3-45)$$

where $\theta_{jm}(x)$ is given by

$$\theta_{jm}(x) = \begin{cases} \frac{\sin[x(\eta_j - \gamma_m)]}{2(\eta_j - \gamma_m)} - \frac{\sin[x(\eta_j + \gamma_m)]}{2(\eta_j + \gamma_m)} & \text{for } \eta_j \neq \gamma_m \\ \frac{x}{2} - \frac{\sin(2\eta_j x)}{4\eta_j} & \text{for } \eta_j = \gamma_m \end{cases} \quad (3-46)$$

The complete solution for this case is given by Equation (3-15) with $C_j(\lambda)$ determined by Equation (3-45).

4.0 PRESSURE PROFILE FOR THE ONE-DIMENSIONAL FINITE-RADIUS MODEL

A schematic diagram of one-dimensional radial flow for a finite DRZ is shown in Figure 2. In comparing Figures 2 and 3, notice that for the one-dimensional model, flow to the drift is neglected. The governing equation for one-dimensional radial flow in a finite DRZ is given by

$$\frac{\partial^2 P}{\partial r^2} + \frac{1}{r} \frac{\partial P}{\partial r} = \frac{1}{\alpha} \frac{\partial P}{\partial t} \quad a \leq r \leq b \quad . \quad (4-1)$$

The conditions on Equation (4-1) for a DRZ of finite radius may be obtained from Equations (2-4) to (2-6), and are given by

$$P = P_0 \quad \text{at } t = 0, \quad a \leq r \leq b \quad (4-2)$$

$$P = 0 \quad \text{at } t > 0, \quad r = a \quad (4-3)$$

$$\frac{\partial P}{\partial r} = 0 \quad \text{at } t > 0, \quad r = b \quad . \quad (4-4)$$

From Equations (2-19) and (2-28), the solution to Equations (4-1) to (4-4) is given by

$$P = \sum_{i=1}^{\infty} C_i \left[Y_0(\lambda_i a) J_0(\lambda_i r) - J_0(\lambda_i a) Y_0(\lambda_i r) \right] \exp \left[-\alpha t \lambda_i^2 \right] \quad (4-5)$$

where λ_i is determined from Equation (2-20), and C_i are constants.

To determine C_i , evaluate Equation (4-5) at $t = 0$, substitute Equation (4-2), multiply both side by $rR_p(r)$, integrate from $r = a$ to $r = b$, and use Equation (2-31) to obtain

$$C_i = \frac{P_0 \int_a^b r R_i(r) dr}{\int_a^b r R_i^2(r) dr} \quad (4-6)$$

Substituting Equations (2-41) and (2-45) into Equation (4-6) results in

$$C_i = \frac{\pi P_0 J_1^2(\lambda_i b)}{J_1^2(\lambda_i b) - J_0^2(\lambda_i a)} \quad (4-7)$$

Substituting Equation (4-7) into Equation (4-5) results in the solution to Equations (4-1) to (4-4), which is given by

$$P = \sum_{i=1}^{\infty} \frac{\pi P_0 J_1^2(\lambda_i^2 b) \exp[-\alpha t \lambda_i^2]}{[J_1^2(\lambda_i b) - J_0^2(\lambda_i a)]} \left\{ Y_0(\lambda_i a) J_0(\lambda_i r) - J_0(\lambda_i a) Y_0(\lambda_i r) \right\} \quad (4-8)$$

For one-dimensional radial flow, vertical variations in the DRZ due to mining the drift prior to drilling the borehole cannot be included. Therefore, only the case of constant P_0 is determined for one-dimensional radial flow.

5.0 PRESSURE PROFILE FOR THE ONE-DIMENSIONAL INFINITE-RADIUS MODEL

In the limit as the outer radius of the DRZ approaches infinity, the finite domain shown in Figure 2 reduces to the infinite domain shown in Figure 1. For the infinite domain, the governing equations are given by

$$\frac{\partial^2 P}{\partial r^2} + \frac{1}{r} \frac{\partial P}{\partial r} = \frac{1}{\alpha} \frac{\partial P}{\partial t} \quad a \leq r < \infty \quad (5-1)$$

$$P = P_0 \quad \text{at } t = 0, \quad a \leq r < \infty \quad (5-2)$$

$$P = 0 \quad \text{at } t > 0, \quad r = a \quad (5-3)$$

$$P = P_0 \quad \text{at } t > 0, \quad r \rightarrow \infty \quad (5-4)$$

Using the method of Separation of Variables, assume that the solution to Equations (5-1) to (5-4) is given by

$$P = R(r)T(t) \quad (5-5)$$

where R and T are the radial and temporal eigenfunctions, respectively. Substituting Equation (5-5) into Equation (5-1) results in Equations (3-7) to (3-12) for $R(r)$. However, $T(t)$ is given within a multiplicative constant by

$$T = \exp[-\alpha t \lambda^2] \quad (5-6)$$

Combining Equations (3-11) and (5-6) results in

$$P(r, t) = \int_0^{\infty} C(\lambda) R(\lambda, r) \exp[-\alpha t \lambda^2] d\lambda \quad (5-7)$$

where $C(\lambda)$ is determined at $t = 0$. Substituting Equation (5-2) into Equation (5-7), multiplying both sides by $rR(v,r)$, and integrating over r from a to b results in

$$P_0 \int_a^b rR(v,r) dr = \int_0^\infty C(\lambda) \int_a^b rR(v,r)R(\lambda,r) dr d\lambda \quad (5-8)$$

In the limit as b approaches infinity, Equation (3-19) can be substituted for the integral on the left-hand side of Equation (5-8). The right-hand side of Equation (5-8) can be determined from the right-hand sides of Equations (3-34), (3-39), and (3-40) in the limit as b approaches infinity. Therefore, Equation (5-8) reduces to

$$-\frac{2P_0}{\pi\lambda^2} = \frac{C(\lambda) [Y_0^2(\lambda a) + J_0^2(\lambda a)]}{\lambda} \quad (5-9)$$

Solving Equation (5-9) for $C(\lambda)$, and substituting $C(\lambda)$ into Equation (5-7) results in the solution to Equations (5-1) to (5-4), which is given by

$$P = -\frac{2P_0}{\pi} \int_0^\infty \exp[-\alpha\lambda^2 t] \left[\frac{J_0(\lambda r)Y_0(\lambda a) - Y_0(\lambda r)J_0(\lambda a)}{\lambda [J_0^2(\lambda a) + Y_0^2(\lambda a)]} \right] d\lambda \quad (5-10)$$

This solution agrees with that reported previously (Crank, 1975, p. 87) and has been used to interpret brine inflow data (Nowak and McTigue, 1987; McTigue and Nowak, 1987; Nowak et al., 1988; Finley et al., 1992).

6.0 FLUID PRODUCTION INTO THE BOREHOLE AND INTO THE DRIFT

The previous analyses determine the fluid pressure throughout the DRZ. However, it is the fluid collected in the borehole that is more readily measured, and not the fluid pressure throughout the domain. Because it may be possible to isolate intervals of the borehole for fluid collection, in this section expressions are derived for the fluid collected over an arbitrary interval in the borehole and over an arbitrary time period. From these expressions, an exact solution can be obtained for the brine inflow rate for the two-dimensional model divided by that for the one-dimensional model. This ratio is a function of only a single dimensionless group that can be easily evaluated. This dimensionless group can be used as a conditional test for determining when two-dimensional effects are important, without requiring any computations of fluid pressures or flow rates.

To determine the importance of fluid loss to the drift, an expression is also derived for the fluid-flow rate escaping to the drift as a function of time for the two-dimensional finite-radius model. For long times, the percentage of the flow rate to the borehole approaches a value independent of time or the rock permeability. This asymptote can also be evaluated without solving for the pressure field or the brine inflow rate.

The fluid velocity into the borehole is a function of depth and time. For a homogeneous porous medium, this velocity is given by Darcy's Law,

$$v = \frac{k}{\mu} \left. \frac{\partial P}{\partial r} \right|_{r=a} \quad (6-1)$$

Notice in Equation (6-1) that the flow velocity is in the negative r -direction, and therefore the velocity into the borehole is proportional to the pressure gradient, and not the negative of the gradient. The derivative of $R_i(r)$ with respect to r is needed to determine the gradient of P at $r = a$. Using Equations (2-16), (2-17), (2-19), and (2-40), this derivative is given by

$$\left. \frac{dR_i}{dr} \right|_{r=a} = \lambda_i (J_0(\lambda_i a) Y_1(\lambda_i a) - Y_0(\lambda_i a) J_1(\lambda_i a)) = -\frac{2}{\pi a} \quad (6-2)$$

Therefore,

$$v = \left\{ \begin{array}{l} -\frac{2k}{\pi \mu a} \sum_{i=1}^{\infty} \sum_{j=1}^{\infty} C_{ij} \sin[\eta_j z] \exp[-\alpha t (\lambda_i^2 + \eta_j^2)] \quad \begin{array}{l} \text{(two-dimensional)} \\ \text{(finite-radius)} \end{array} \\ -\frac{2k}{\pi \mu a} \sum_{i=1}^{\infty} C_i \exp[-\alpha t \lambda_i^2] \quad \begin{array}{l} \text{(one-dimensional)} \\ \text{(finite-radius)} \end{array} \\ -\frac{2k}{\pi \mu a} \sum_{j=1}^{\infty} \int_0^{\infty} C_j(\lambda) Z_j(z) \exp[-\alpha t (\lambda^2 + \eta_j^2)] d\lambda \quad \begin{array}{l} \text{(two-dimensional)} \\ \text{(infinite-radius)} \end{array} \\ \frac{4kP_0}{a\mu\pi^2} \int_0^{\infty} \frac{e^{-\alpha\lambda^2 t}}{\lambda [J_0^2(\lambda a) + Y_0^2(\lambda a)]} d\lambda \quad \begin{array}{l} \text{(one-dimensional)} \\ \text{(infinite-radius)} \end{array} \end{array} \right. \quad (6-3)$$

where C_{ij} is given either by Equation (2-47) for P_0 constant, or Equation (2-56) for P_0 varying with depth, C_i is given by Equation (4-7) for one-dimensional flow with a finite DRZ, and $C_j(\lambda)$ is given by either Equation (3-42) or (3-45). The fluid velocity for the one-dimensional infinite-radius model is obtained from Equations (5-10), (6-1), and (6-2) and agrees with the solution reported in the literature (Crank, 1975, p. 87).

The flow rate into the borehole over the depth interval L_1 to L_2 can be determined by integrating the velocity over the cylindrical surface of the interval in the borehole, and is given by

$$F = 2\pi a \int_{L_1}^{L_2} v \, dz \quad \text{for } 0 \leq L_1 < L_2 \leq L \quad (6-4)$$

F can be determined by substituting Equation (6-3) into Equation (6-4) to obtain

$$F = \left\{ \begin{array}{l} \frac{4k}{\mu} \sum_{i=1}^{\infty} \sum_{j=1}^{\infty} \left[\frac{C_{ij} [\cos(\eta_j L_2) - \cos(\eta_j L_1)]}{\eta_j} \right] \exp\left[-\alpha t (\lambda_i^2 + \eta_j^2)\right] \\ \hspace{20em} \text{(two-dimensional)} \\ \hspace{20em} \text{(finite-radius)} \\ \\ \frac{4k(L_1 - L_2)}{\mu} \sum_{i=1}^{\infty} C_i \exp\left[-\alpha t \lambda_i^2\right] \\ \hspace{20em} \text{(one-dimensional)} \\ \hspace{20em} \text{(finite-radius)} \\ \\ \frac{4k}{\mu} \sum_{j=1}^{\infty} \int_0^{\infty} \left[\frac{C_j(\lambda) [\cos(\eta_j L_2) - \cos(\eta_j L_1)]}{\eta_j} \right] \exp\left[-\alpha t (\lambda^2 + \eta_j^2)\right] d\lambda \\ \hspace{20em} \text{(two-dimensional)} \\ \hspace{20em} \text{(infinite-radius)} \\ \\ \frac{8kP_0(L_2 - L_1)}{\mu\pi} \int_0^{\infty} \frac{e^{-\alpha \lambda^2 t}}{\lambda [J_0^2(\lambda a) + Y_0^2(\lambda a)]} d\lambda \\ \hspace{20em} \text{(one-dimensional)} \\ \hspace{20em} \text{(infinite-radius)} \end{array} \right. \quad (6-5)$$

The integrands for an infinite domain given in Equation (6-5) are singular for $\lambda = 0$. Therefore, for numerical computation of the integral, D. McTigue (Sandia National Laboratories, Department 1513) has developed a scheme that splits the integral into two parts. The first part of the integral is evaluated analytically over the domain $\lambda = 0$ to $\lambda = \epsilon$, as $\epsilon \rightarrow 0$. The second part of the integral is evaluated numerically from $\lambda = \epsilon$ to $\lambda \rightarrow \infty$. The upper limit of the second part of the integral is determined by increasing this limit until the value of the integral converges. A

derivation of McTigue's method for analytical integration of the first part of the integral is given in Appendix B.

If the initial pressure profile is depth-dependent, such as in the case when there is much time between mining the drift and drilling the borehole, then a two-dimensional model is appropriate. However, for a constant initial pressure, the one-dimensional flow rates may be comparable to those calculated with the two-dimensional model. A quantitative conditional test for determining if two-dimensional effects are important can be developed from Equation (6-5), for constant $P_0 = P_\infty - P_a$. In this case, the ratio of the fluid production rates over the entire borehole for the two-dimensional model divided by that for the one-dimensional model is given by

$$\frac{F_{2D}}{F_{1D}} = \frac{8}{\pi^2} \sum_{j=1}^{\infty} \frac{\exp\left[-\frac{4\alpha t}{L^2} \frac{(2j-1)^2 \pi^2}{16}\right]}{(2j-1)^2} \quad L_1 = 0, L_2 = L \quad (6-6)$$

Equation (6-6) is valid regardless of the DRZ outer radius, as long as the same outer radius is used in determining F_{2D} and F_{1D} . For $\alpha t/L^2 = 0$, the summation in Equation (6-6) reduces to $\pi^2/8$. Thus in this limit, the production rates for one- and two-dimensional models are identical. As expected, as $L \rightarrow \infty$, the two-dimensional brine inflow rate approaches the inflow rate for the one-dimensional model. However, for a positive value of $\alpha t/L^2$, the summation is less than $\pi^2/8$. Therefore, compared to the two-dimensional model with the same DRZ outer radius, the one-dimensional model always overestimates the flow rate to the borehole.

In Equation (6-6) the term $4\alpha t$ is defined in this work to be equal to the square of the penetration depth, D_p . The penetration depth is a measure of how far significant depressurization has traveled into the DRZ away from the borehole, or from the drift. This concept will be explained in much greater detail in Section 8.1. From the definition

$$D_p^2 = 4\alpha t, \quad (6-7)$$

Equation (6-6) can be expressed as

$$\frac{F_{2D}}{F_{1D}} = \frac{8}{\pi^2} \sum_{j=1}^{\infty} \frac{\exp \left[- \frac{D_p^2}{L^2} \frac{(2j-1)^2 \pi^2}{16} \right]}{(2j-1)^2} \quad L_1 = 0, L_2 = L \quad (6-8)$$

A plot of Equation (6-8) is given in Figure 5.

From this analysis, D_p/L is the important criterion, not L/a , for determining if two-dimensional effects are important. The larger D_p/L , the greater the importance of two-dimensional effects. The test for the one-dimensional solution for the brine inflow rate, to be within 5 or 50% of that for the two-dimensional solution, requires D_p/L to be less than 0.0886 or 0.887, respectively. By rearranging Equation (6-7) and substituting Equation (2-2), this test sets an upper bound on the time over which the one-dimensional solution may be used for a specified percentage agreement with the two-dimensional solution. Thus, the conditional test can be expressed as a maximum time that one- and two-dimensional models agree, and is given by

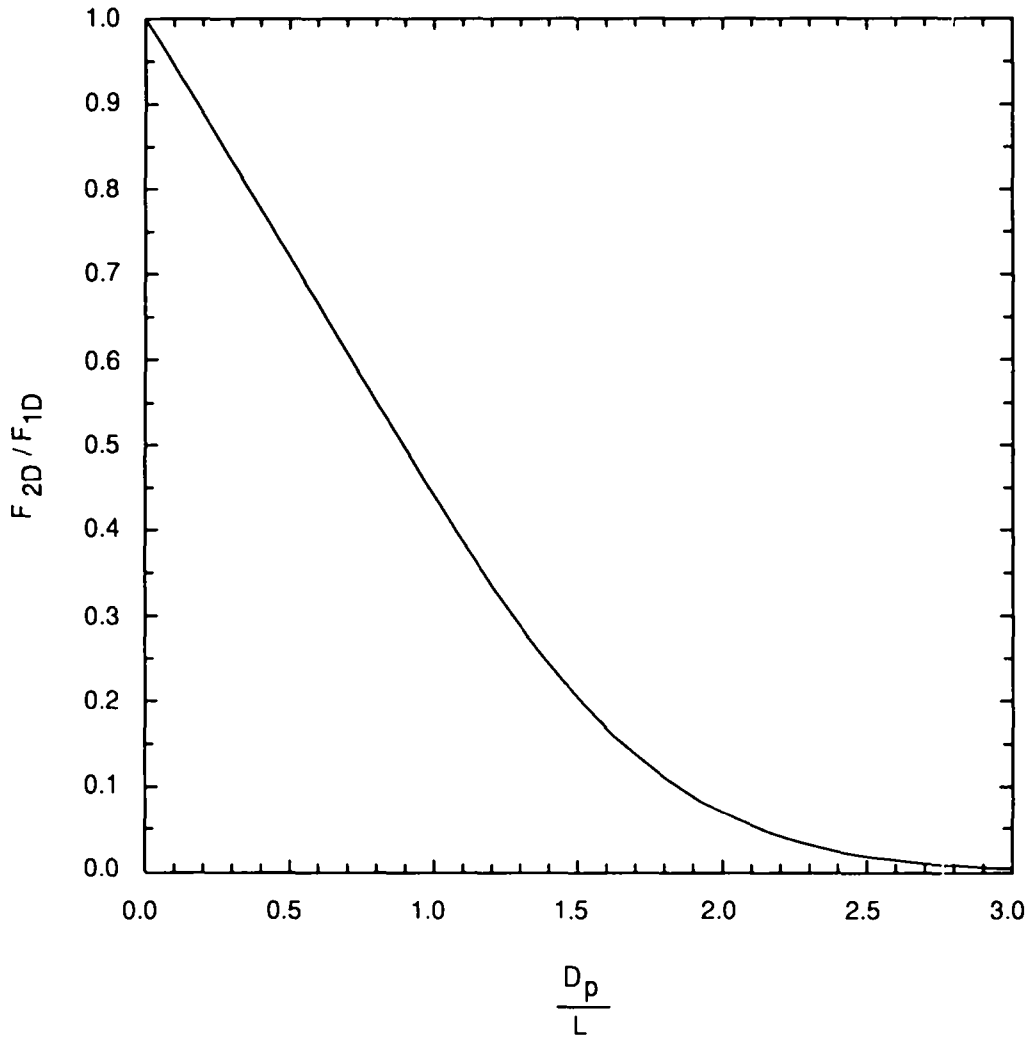
$$t_{\max} = \frac{[D_p/L]_*^2 \mu [\phi c_f + c_r] L^2}{4k} \quad (6-9)$$

where $[D_p/L]_*$ given in Equation (6-9) may be, for example, either 0.0886 or 0.887 for 5 or 50% agreement, respectively, between the two- and one-dimensional flow rates.

The fluid velocity into the drift depends on r and is given by

$$u = \frac{k}{\mu} \frac{\partial P}{\partial z} \Big|_{z=0} \quad (6-10)$$

From Equations (2-29) and (3-15), this velocity is given respectively by



TRII-6119-16-0

Figure 5. Flow rate to the borehole for two-dimensional models divided by the flow rate to the borehole for one-dimensional models, for the same DRZ outer radius, as a function of the penetration depth divided by the borehole length, for constant initial pressure in the DRZ.

$$u = \left\{ \begin{array}{l} \frac{k}{\mu} \sum_{i=1}^{\infty} \sum_{j=1}^{\infty} C_{ij} \eta_j R_i \exp\left[-\alpha t[\lambda_i^2 + \eta_j^2]\right] \\ \hspace{15em} \text{(two-dimensional)} \\ \hspace{15em} \text{(finite-radius)} \\ \\ \frac{k}{\mu} \sum_{j=1}^{\infty} \int_0^{\infty} C_j(\lambda) \eta_j R(\lambda, r) \exp\left[-\alpha t[\lambda^2 + \eta_j^2]\right] d\lambda \\ \hspace{15em} \text{(two-dimensional)} \\ \hspace{15em} \text{(infinite-radius)} \end{array} \right. \quad (6-11)$$

The flow rate into the drift can be determined by integrating the velocity over the surface area of the DRZ that is bounded by the drift and is given by

$$f = 2\pi \int_a^b ru \, dr \quad (6-12)$$

Substituting Equation (6-11) into Equation (6-12) for the two-dimensional finite-radius model and using Equation (2-41) results in

$$f = -\frac{4k}{\mu} \sum_{i=1}^{\infty} \sum_{j=1}^{\infty} \frac{C_{ij} \eta_j}{\lambda_i^2} \exp\left[-\alpha t[\lambda_i^2 + \eta_j^2]\right] \quad \begin{array}{l} \text{(two-dimensional)} \\ \text{(finite-radius)} \end{array} \quad (6-13)$$

The percentage of the flow rate to the borehole is given by

$$F_{\%} = \frac{100F}{F + f} \quad (6-14)$$

where F and f are given by Equations (6-5) and (6-13), respectively. For the two-dimensional finite-radius model, F_g must be close to 100 for flow to the drift to be unimportant.

A simple expression for F_g may be obtained for long times, such that only the first term is required in the eigenfunction expansions for F and f . In this limit, F_g is given by

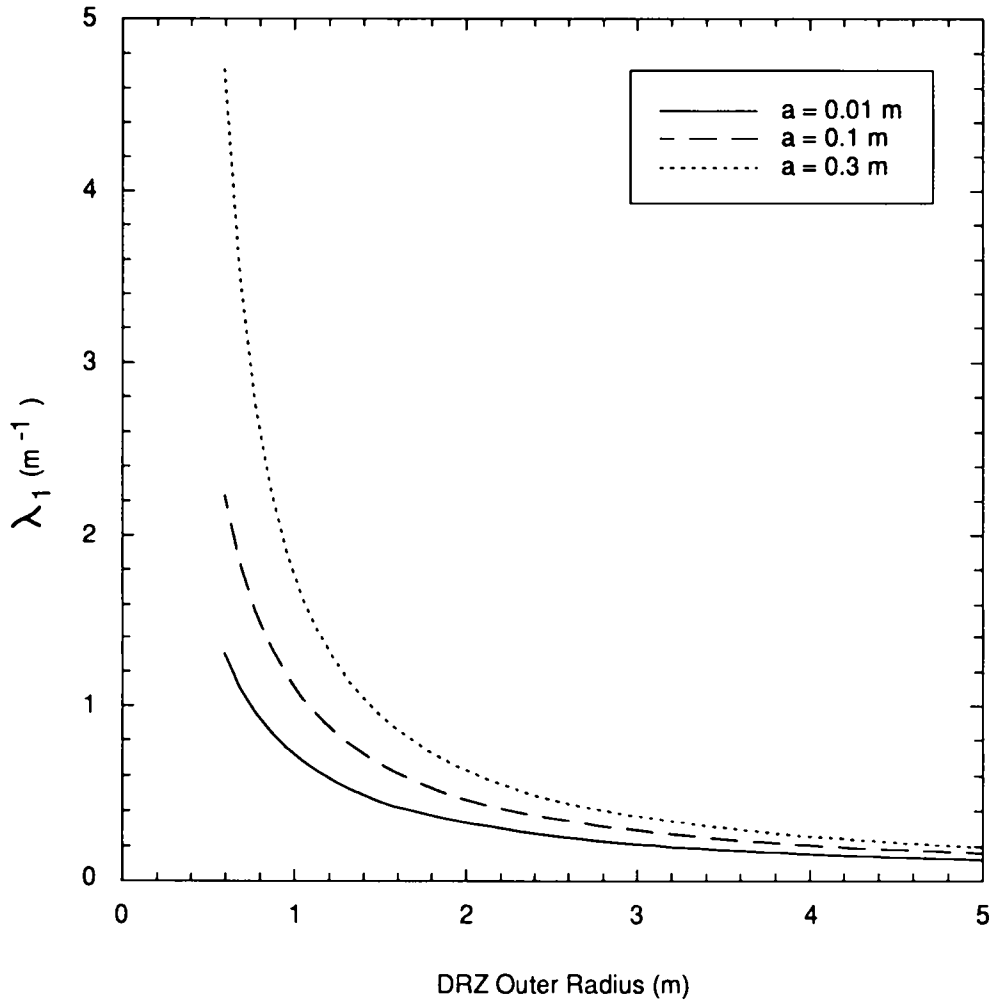
$$F_g = \frac{100\lambda_1^2}{\lambda_1^2 + \eta_1^2} \quad \text{for} \quad \alpha t \lambda_1^2 \gg 1, \quad \text{and} \quad \alpha t \eta_1^2 \gg 1 \quad (6-15)$$

where λ_1 and η_1 are given by Equations (2-20) and (2-26), respectively. A major advantage of using Equation (6-15) is that F_g reduces to a function of only three geometric parameters (a , b , and L). F_g will be close to 100, and thus flow to the drift will be unimportant if the following condition is satisfied:

$$\eta_1^2 \ll \lambda_1^2 \quad \text{for} \quad \alpha t \lambda_1^2 \gg 1, \quad \text{and} \quad \alpha t \eta_1^2 \gg 1 \quad (6-16)$$

As is shown in Section 8.2 for parameters typical of the WIPP, even for short time scales on the order of days, Equation (6-16) provides a good upper estimate of the percentage of the flow rate to the borehole.

For checking the condition given in Equation (6-16), η_1 can be determined from Equation (2-26) and is given by $\pi/(2L)$. The first radial eigenvalue, λ_1 , is the solution to Equation (2-20) for $i = 1$ and can be determined numerically using the method given in Appendix A. For convenience, λ_1 is given in Figure 6 for a range of inner and outer DRZ radii. Notice that η_1 is inversely proportional to L . Therefore, flow to the drift becomes less important as the borehole depth increases. This observation agrees with what one would expect; however, Equations (6-14) and (6-16) provide a quantitative basis for determining the length of the borehole required to neglect flow to the drift.



TRIF-6119-17-0

Figure 6. First radial eigenvalue as a function of the DRZ inner radius a , and the DRZ outer radius b . This plot is a solution of Equation (2-20) for $i = 1$.

7.0 CUMULATIVE FLUID PRODUCTION

The cumulative fluid volume collected in the borehole from time t_1 to t_2 from depths L_1 to L_2 is given by

$$\bar{F} = \int_{t_1}^{t_2} F dt \quad \text{for } 0 \leq t_1 < t_2 \quad (7-1)$$

Substituting Equation (6-5) into Equation (7-1) for finite DRZs results in

$$\bar{F} = \left\{ \begin{array}{l} \frac{4k}{\alpha\mu} \sum_{i=1}^{\infty} \sum_{j=1}^{\infty} \frac{C_{ij} [\cos(\eta_j L_1) - \cos(\eta_j L_2)]}{\eta_j (\lambda_i^2 + \eta_j^2)} \times \\ \quad \left[\exp[-\alpha t_2 (\lambda_i^2 + \eta_j^2)] - \exp[-\alpha t_1 (\lambda_i^2 + \eta_j^2)] \right] \\ \quad \text{(two-dimensional)} \\ \quad \text{(finite-radius)} \\ \\ \frac{4k(L_2 - L_1)}{\alpha\mu} \sum_{i=1}^{\infty} \frac{C_i}{\lambda_i^2} \left[\exp[-\alpha t_2 \lambda_i^2] - \exp[-\alpha t_1 \lambda_i^2] \right] \\ \quad \text{(one-dimensional)} \\ \quad \text{(finite-radius)} \end{array} \right. \quad (7-2)$$

The cumulative fluid volume produced over the entire borehole up to time t_2 may be determined directly from Equation (7-2) and is given by

$$\bar{F} = \begin{cases} \frac{4k}{\alpha\mu} \sum_{i=1}^{\infty} \sum_{j=1}^{\infty} \frac{C_{ij}}{\eta_j(\lambda_i^2 + \eta_j^2)} \left(\exp \left[-\alpha t_2 (\lambda_i^2 + \eta_j^2) \right] - 1 \right) & \begin{array}{l} \text{(two-dimensional)} \\ \text{(finite-radius)} \\ (L_1=0, L_2=L, t_1=0) \end{array} \\ \frac{4kL}{\alpha\mu} \sum_{i=1}^{\infty} \frac{C_i}{\lambda_i^2} \left(\exp \left[-\alpha t_2 \lambda_i^2 \right] - 1 \right) & \begin{array}{l} \text{(one-dimensional)} \\ \text{(finite-radius)} \\ (L_1=0, L_2=L, t_1=0) \end{array} \end{cases} \quad (7-3)$$

The cumulative fluid volume escaping into the drift from time t_1 to t_2 is given by

$$\bar{f} = \int_{t_1}^{t_2} f \, dt \quad \text{for } 0 \leq t_1 < t_2 \quad (7-4)$$

Substituting Equation (6-13) into Equation (7-4) results in

$$\bar{f} = \frac{4k}{\alpha\mu} \sum_{i=1}^{\infty} \sum_{j=1}^{\infty} \frac{\eta_j C_{ij}}{\lambda_i^2 (\lambda_i^2 + \eta_j^2)} \left(\exp \left[-\alpha t_2 (\lambda_i^2 + \eta_j^2) \right] - \exp \left[-\alpha t_1 (\lambda_i^2 + \eta_j^2) \right] \right) \quad (7-5)$$

For one-dimensional radial flow, u , f , and \bar{f} are zero because there is no flow in the vertical direction. As will be shown in Section 8.2, even for values of $b/L < 1$, the one-dimensional approximation can neglect the dominant fluid flow path out of the DRZ.

For a finite DRZ, the total fluid volume that will be produced is given by the sum $\bar{f} + \bar{F}$ in the limit as $t_2 \rightarrow \infty$. From Equations (7-3) and (7-5) this limit is given by

$$\bar{F} + \bar{f} = \begin{cases} -\frac{4k}{\alpha\mu} \sum_{i=1}^{\infty} \sum_{j=1}^{\infty} \frac{C_{ij}}{\lambda_i^2 + \eta_j^2} \left(\frac{1}{\eta_j} + \frac{\eta_j}{\lambda_i^2} \right) & \begin{array}{l} \text{(two-dimensional, finite-radius)} \\ (L_1 = 0, L_2 = L, t_1 = 0, t_2 \rightarrow \infty) \end{array} \\ -\frac{4kL}{\alpha\mu} \sum_{i=1}^{\infty} \frac{C_i}{\lambda_i^2} & \begin{array}{l} \text{(one-dimensional, finite-radius, } \bar{f} = 0) \\ (L_1 = 0, L_2 = L, t_1 = 0, t_2 \rightarrow \infty) \end{array} \end{cases} \quad (7-6)$$

If the rock compressibility is neglected (i.e., $c_r = 0$), for constant $P_0(z) = P_\infty - P_a$, this limiting total fluid volume produced from the DRZ can also be determined directly from the definition of fluid compressibility, which is given by

$$c_f = \frac{1}{\rho} \frac{d\rho}{dP} \quad (7-7)$$

where ρ is the fluid density. Integrating Equation (7-7) from ambient conditions (which are denoted by the subscript a) to far-field conditions (which are denoted by the subscript ∞), the fluid density at ambient conditions is given by

$$\rho_a = \rho_\infty \exp \left[c_f (P_a - P_\infty) \right] \quad (7-8)$$

The total pore space in the DRZ is given by

$$V = \phi L \pi (b^2 - a^2) \quad (7-9)$$

This is the space occupied by the fluid initially. In the limit as $t_2 \rightarrow \infty$, all the fluid will be at pressure P_a and thus have a density ρ_a . In this

limit, the total space occupied by the fluid is $\Delta + V$, where Δ is the incremental space the fluid occupies due to depressurization to ambient conditions. Because the fluid mass is the same before and after depressurization, Equation (7-8) can be expressed as

$$\frac{1}{V+\Delta} = \frac{1}{V} \exp\left[c_f(P_a - P_\infty)\right] \quad (7-10)$$

From Equation (7-10) the incremental fluid space can be determined, and is equal to the total fluid volume produced into the borehole plus the fluid volume escaping into the drift. Thus,

$$\left. \begin{array}{l} (\bar{F} + \bar{f}) \\ t_2 \rightarrow \infty \\ t_1 = 0 \\ L_1 = 0 \\ L_2 = L \\ P_0 = P_\infty - P_a \\ c_r = 0 \end{array} \right\} = \Delta = \phi\pi L \left[b^2 - a^2 \right] \left(\exp\left[c_f [P_\infty - P_a] \right] - 1 \right) \quad (7-11)$$

Equation (7-11) provides a convenient independent check on Equation (7-6).

8.0 SAMPLE CALCULATIONS

The solutions given previously are in terms of infinite series eigenfunction expansions. Although these are exact solutions, from the equations it is very difficult to gain an appreciation of the behavior of the solutions. Therefore, several sample calculations are presented in Sections 8.1 and 8.2. To present a manageable number of cases for comparison, the following parameters are held constant for all the sample calculations:

$$\phi = \text{rock porosity} = 0.01$$

$$c_f = \text{fluid compressibility [from Rechard et al., 1991]} = 2.5 \times 10^{-10} \text{ Pa}^{-1}$$

$$c_r = \text{rock compressibility} = 4.8 \times 10^{-12} \text{ Pa}^{-1}$$

$$L = \text{borehole length} = 3.0 \text{ m}$$

$$a = \text{borehole radius} = \text{DRZ inner radius} = 0.05 \text{ m}$$

$$P_\infty = \text{fluid pressure in undisturbed rock} = 11 \times 10^6 \text{ Pa}$$

$$P_a = \text{ambient pressure in borehole and in drift} = 0.1 \times 10^6 \text{ Pa}$$

$$\mu = \text{fluid viscosity} = 0.0016 \text{ Pa}\cdot\text{s}.$$

The values chosen correspond to conditions in halite at the WIPP Site. It had been anticipated that if the ratio $L/a \gg 1$, the flow would be predominantly one-dimensional. However, as shown in Section 6.0, this ratio is not the appropriate one to use for assessing the importance of two-dimensional effects. Further, the results in Sections 8.1 and 8.2 show that even with $L/a = 60$, there are still significant two-dimensional effects.

Two-dimensional effects can influence the solution through a depth-dependent initial condition resulting from mining the drift and through fluid escaping to the floor of the drift after drilling the borehole. One-dimensional models cannot incorporate a depth-dependent initial condition. Therefore, in the first two sets of sample calculations, the initial fluid pressure is constant so that one- and two-dimensional models may be compared for the same initial conditions. Thus, the two-dimensional effect discussed in these sample calculations is a result of only neglecting flow to the drift during brine flow to the borehole. A summary of the sets of sample calculations is given in Table 2.

Table 2. Sample Calculations

Figure	Plot Type*	Parameters
7	Two-Dimensional Contours of $(P_f - P_a)/(P_\infty - P_a)$	Penetration Depth = $2(\alpha t)^{1/2} = 0.2$ m DRZ outer radius = $b = 1.0$ m
8	Two-Dimensional Contours of $(P_f - P_a)/(P_\infty - P_a)$	Penetration Depth = $2(\alpha t)^{1/2} = 1.0$ m DRZ outer radius = $b = 1.0$ m
9	Two-Dimensional Contours of $(P_f - P_a)/(P_\infty - P_a)$	Penetration Depth = $2(\alpha t)^{1/2} = 3.0$ m DRZ outer radius = $b = 1.0$ m
10	Two-Dimensional Contours of $(P_f - P_a)/(P_\infty - P_a)$	Penetration Depth = $2(\alpha t)^{1/2} = 1.0$ m DRZ outer radius = $b = 3.0$ m
11	Two-Dimensional Contours of $(P_f - P_a)/(P_\infty - P_a)$	Penetration Depth = $2(\alpha t)^{1/2} = 3.0$ m DRZ outer radius = $b = 3.0$ m
12	Brine Inflow Rates For All Four Models	Rock Permeability = $k = 10^{-20}$ m ²
13	Brine Inflow Rates For All Four Models	Rock Permeability = $k = 10^{-21}$ m ²
14	Brine Inflow Rates For All Four Models	Rock Permeability = $k = 10^{-22}$ m ²
15	Percentage of Flow to Borehole for Two-Dimensional Finite-Radius Model	
16	Brine Inflow Rates For All Four Models	Rock Permeability = $k = 10^{-20}$ m ² DRZ depth = $H = 3.0$ m Time period between mining drift and drilling borehole = $\tau = 1$ year

Table 2. Sample Calculations (continued)

Figure	Plot Type*	Parameters
17	Brine Inflow Rates For All Four Models	Rock Permeability = $k = 10^{-21} \text{ m}^2$ DRZ depth = $H = 3.0 \text{ m}$ Time period between mining drift and drilling borehole = $\tau = 1 \text{ year}$
18	Brine Inflow Rates For All Four Models	Rock Permeability = $k = 10^{-22} \text{ m}^2$ DRZ depth = $H = 3.0 \text{ m}$ Time period between mining drift and drilling borehole = $\tau = 1 \text{ year}$

*Notation

P_f = fluid pressure

P_a = ambient pressure in borehole and in drift

P_∞ = fluid pressure in undisturbed rock far from drift or borehole

In the first set of sample calculations, contours of $(P_f - P_a)/(P_\infty - P_a)$, a dimensionless pressure as determined from Equation (2-49) are given for different values of b , the outer radius of the DRZ. The objective of these calculations is to display depressurization of the region due to brine escaping into the drift and flowing into the borehole.

The second set of solutions presents borehole brine inflow rates for all four models (i.e., one-dimensional infinite-radius, one-dimensional finite-radius, two-dimensional finite-radius models, and two-dimensional infinite-radius), for different values of k , the permeability, and b , the outer radius of the DRZ. By comparing results from different models, the effects of neglecting flow to the drift are highlighted. To further display these effects, a plot showing the percentage of the flow to the borehole for the two-dimensional finite-radius model is given.

The two-dimensional effect of mining the drift one year before drilling the borehole is presented in the third set of sample calculations. In these calculations, except for τ , all the parameters are identical to those used in the second set of calculations. Thus, by comparing the second and third sets of calculations, the effect of prior depressurization can be displayed. This effect is not included in one-dimensional models.

For the calculations, the functions J_0 , Y_0 , J_1 , and Y_1 are determined using polynomial approximations (Abramowitz and Stegun, 1970, pp. 369-370, Eqs. 9.4.1-9.4.6). These are the only Bessel functions required to compute the solutions for the pressure contours and the brine inflow rates. All infinite series are summed until the partial sums converge to within three significant figures. As noted after Equation (2-48), double summations can be avoided because they factor into a product of two summations as given by Equation (2-49). This simplification greatly reduces computer time and is also used for evaluating the double summation in Equation (6-5). The integrals for the infinite-radius models are calculated using the method discussed after Equation (6-5) and in Appendix B. For this calculation, ϵ is 10^{-6} m^{-1} , and the second part of the integral is computed using an adaptive Gauss-Legendre quadrature technique.

8.1 Sample Calculations of Two-Dimensional Contours of the Dimensionless Pressure

The two-dimensional finite-radius solution for constant initial pressure in the DRZ is given by Equation (2-49). For this case, the fluid pressure throughout the DRZ is initially P_∞ , and at time just greater than zero, the drift is mined and a borehole drilled such that at both of these locations the pressure is at P_a . Under these conditions, the fluid pressure is determined by the following 13 parameters, collected into four sets:

- The DRZ geometry: a , b , and L
- The physical properties of the halite: c_r , ϕ , and k
- The physical properties of the brine: c_f and μ
- The spatial position, time, and pressures: r , z , t , P_a , and P_∞ .

From Equation (2-49) this list of 13 parameters can be grouped to only seven parameters: r , z , L , αt , a , b , and $(P_f - P_a)/(P_\infty - P_a)$, where α is defined in Equation (2-2). Because the DRZ inner radius a , and the borehole length L , are held constant in the sample calculations, there are five free parameters given by r , z , αt , b , and $(P_f - P_a)/(P_\infty - P_a)$. Thus, a contour plot of the dimensionless pressure, given by $(P_f - P_a)/(P_\infty - P_a)$, as a function of r and z , is determined by specifying the two parameters, αt and b . This reduction in complexity is used in the following analysis.

Instead of discussing the solution for the fluid pressure minus the ambient pressure, given by P , based on the above analysis, it is more convenient to cast the problem in terms of the dimensionless pressure, $(P_f - P_a)/(P_\infty - P_a)$. Initially, the dimensionless pressure is 1 throughout the DRZ. The system is abruptly disturbed by instantaneously dropping the dimensionless pressure in the drift and in the borehole to 0. (In reality of course, mining the drift and drilling a borehole cannot be performed instantaneously. Rather, these conditions are applied when the time to perform these operations is much shorter than the time between completing both operations and measuring the brine inflow rate.) For a fixed DRZ outer radius b , a contour plot of the dimensionless pressure will evolve determined only by the parameter group αt . For convenience, this group can be used to define a penetration depth given by,

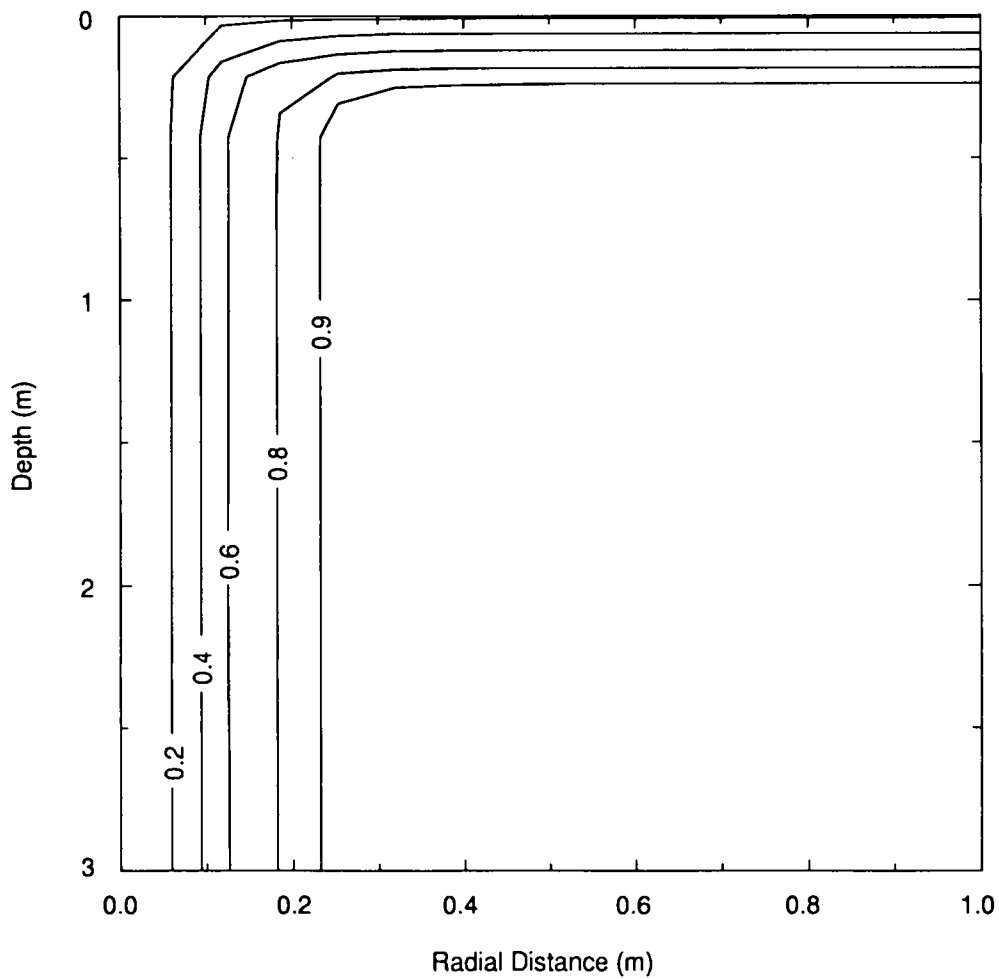
$$D_p = 2\sqrt{\alpha t} = \sqrt{\frac{4kt}{\mu[\phi c_f + c_r]}} \quad (8-1)$$

The penetration depth is a measure of how far a disturbance in pressure will propagate into the region. In the sample calculations, the disturbance is the drop in pressure created in the borehole and in the drift. If at a location in the DRZ, the distance to either the borehole or the drift floor is much less than the penetration depth, then significant depressurization can be expected at this location. Similarly, if the location is much farther from the drift or the borehole than the penetration depth, then to a good approximation the pressure at this location will not have yet been affected by depressurization. Because the penetration depth increases with time, all

locations in the DRZ a finite distance from the borehole or the drift floor will eventually be affected by depressurization.

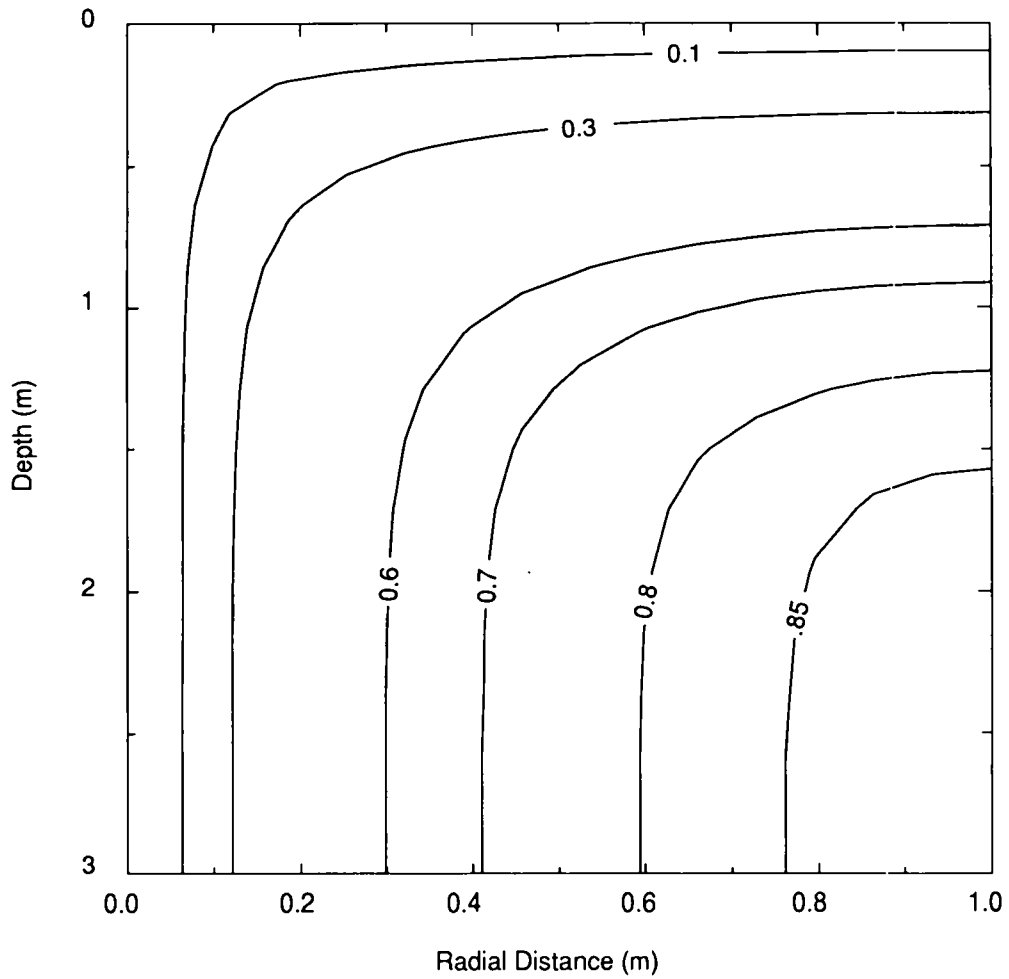
To demonstrate the utility of the penetration depth concept, contours of the dimensionless pressure in the DRZ determined from Equation (2-49) are shown in Figure 7 for a DRZ with an outer radius of 1.0 m and a penetration depth of 0.2 m. Using Equation (8-1), and the parameters μ , c_f , c_r , and ϕ specified in Section 8.0, this penetration depth corresponds to a value of $kt = 1.2 \times 10^{-16} \text{ m}^2 \cdot \text{s}$. Thus, if the DRZ permeability is 10^{-21} m^2 , then a penetration depth of 0.2 m corresponds to a time of $1.2 \times 10^5 \text{ s}$, or 32 hours. Similarly, for a permeability of 10^{-20} m^2 , the penetration depth would correspond to a time of $1.2 \times 10^4 \text{ s}$, or 3.2 hours. Notice that since $D_p \ll b-a$, and $D_p \ll L$, there are hardly any pressure changes in the region that is near the outer radius and the bottom of the DRZ. Nearly all the changes in pressure are confined to a small region adjacent to the borehole and the drift. As the penetration depth increases to 1.0 m (as shown in Figure 8), much of the DRZ, which extends to a radius of 1.0 m, is now affected. For a permeability of 10^{-21} m^2 , this greater penetration depth corresponds to a time of 34 days. Figure 9 shows that for much longer times, corresponding to a penetration depth of 3.0 m, which is much greater than the outer radius of the DRZ, the pressure throughout the DRZ decays to a very small percentage of the original pressure. For a permeability of 10^{-21} m^2 , this penetration depth would correspond to a time of 304 days.

For larger DRZ outer radii, the penetration depth needs to be longer, so that the effects of depressurizing the borehole reach the outer radius of the DRZ. If the outer radius of the DRZ had been 3.0 m, instead of 1.0 m as in Figure 8, then much less of the region would have been depressurized. This is shown in Figure 10, where the outer radius of the DRZ is 3.0 m and the penetration depth is 1.0 m. Comparing Figures 8 and 10, in Figure 10 with the larger DRZ outer radius, pressure changes have not yet significantly reached the outer boundaries of the DRZ. However, for longer times, as shown in Figure 11 for a penetration depth of 3.0 m, much of the DRZ is affected.



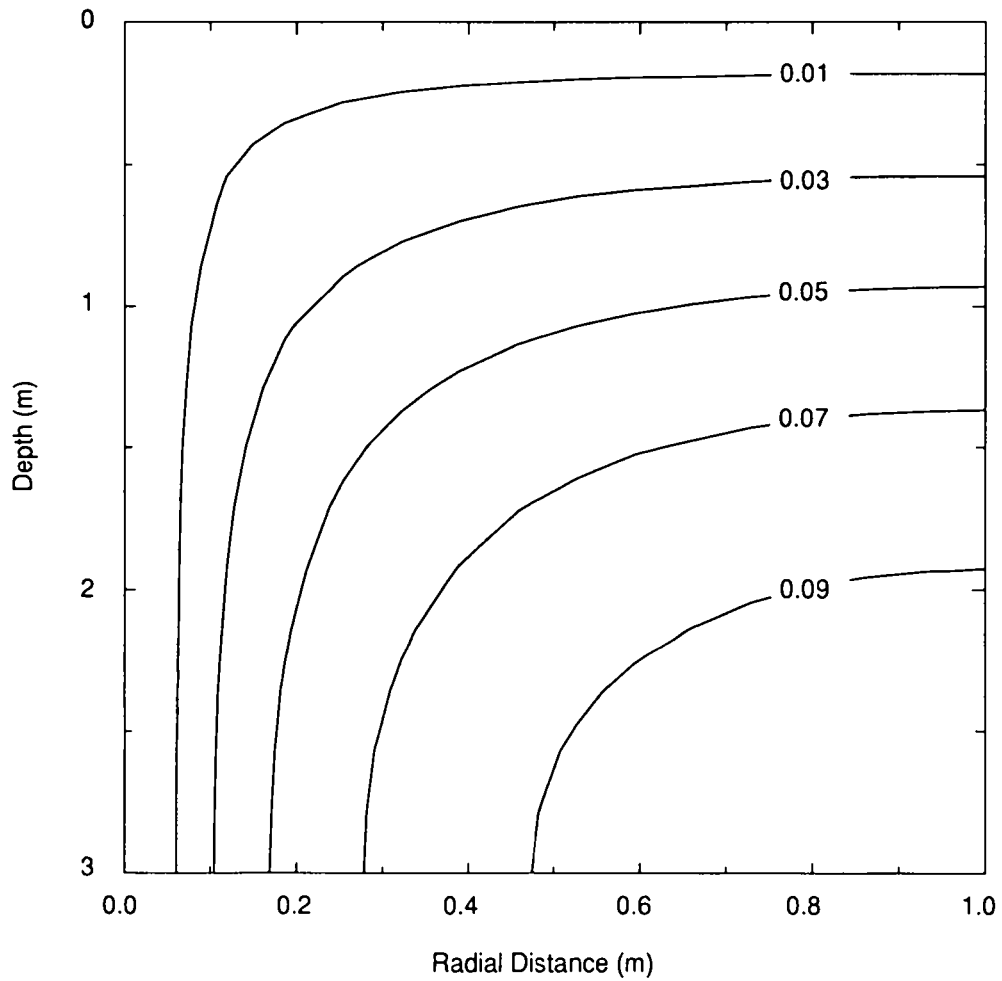
TRIF-6119-2-0

Figure 7. Dimensionless pressure contours of $(P_f - P_a)/(P_\infty - P_a)$ at a penetration depth of $D_p = 0.2$ m, for a borehole with DRZ inner and outer radii of $a = 0.05$ m and $b = 1.0$ m, respectively, and a borehole length of $L = 3.0$ m.



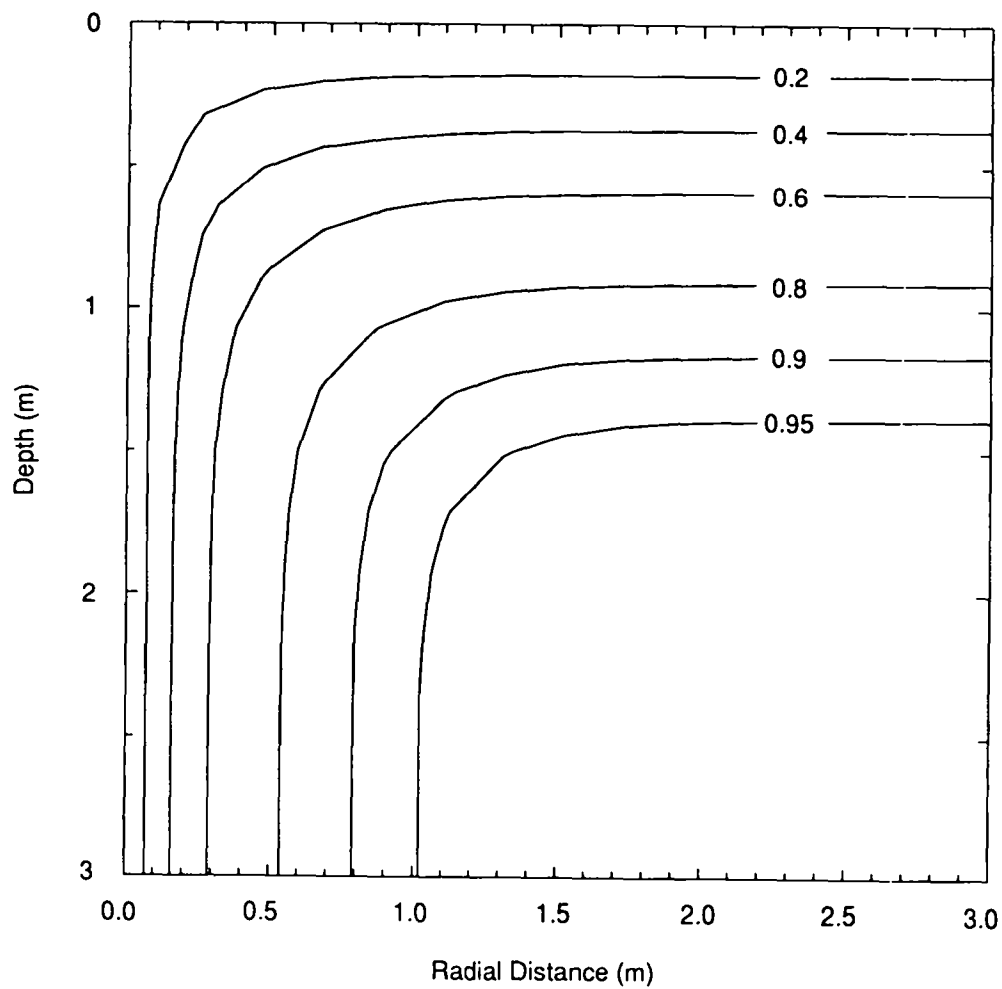
TRIF-6119-4-0

Figure 8. Dimensionless pressure contours of $(P_f - P_a)/(P_\infty - P_a)$ at a penetration depth of $D_p = 1.0$ m, for a borehole with DRZ inner and outer radii of $a = 0.05$ m and $b = 1.0$ m, respectively, and a borehole length of $L = 3.0$ m.



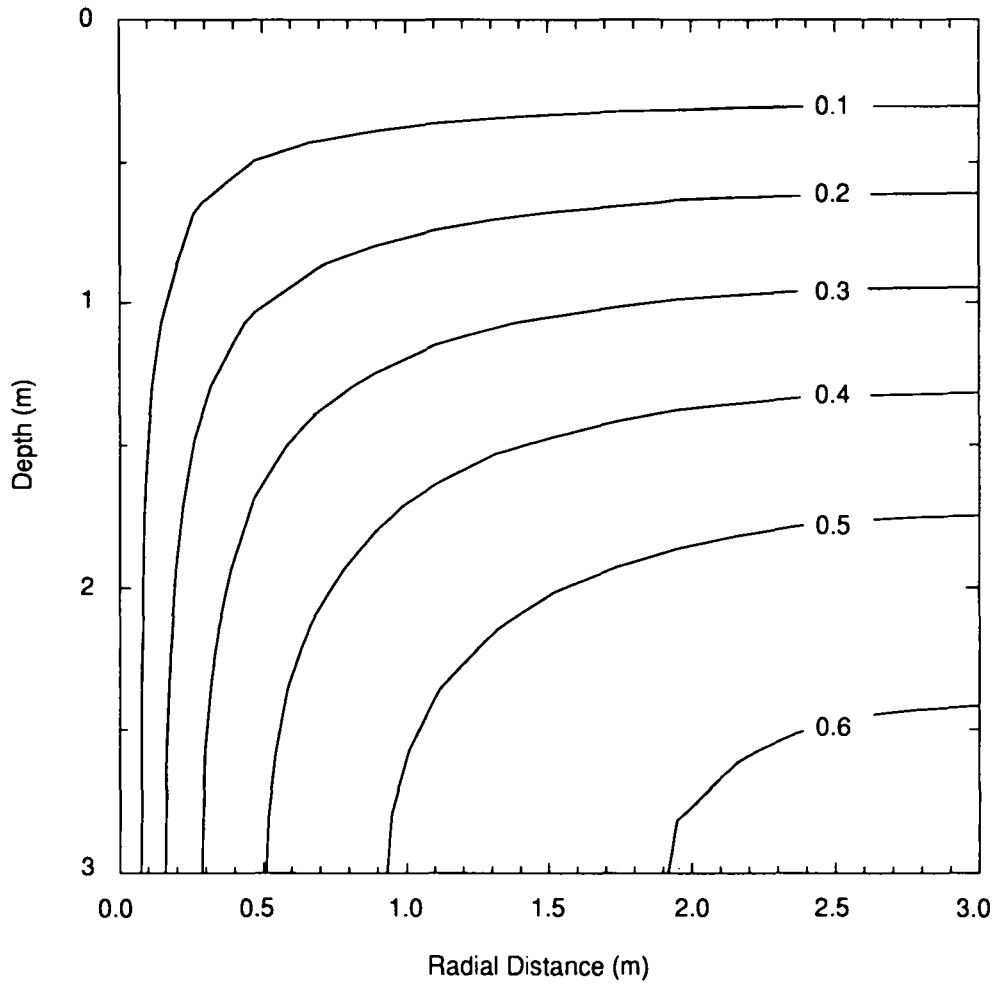
TRIF-6119-5-0

Figure 9. Dimensionless pressure contours of $(P_f - P_a)/(P_\infty - P_a)$ at a penetration depth of $D_p = 3.0$ m, for a borehole with DRZ inner and outer radii of $a = 0.05$ m and $b = 1.0$ m, respectively, and a borehole length of $L = 3.0$ m.



TRIF-6119-6-0

Figure 10. Dimensionless pressure contours of $(P_f - P_a)/(P_\infty - P_a)$ at a penetration depth of $D_p = 1.0$ m, for a borehole with DRZ inner and outer radii of $a = 0.05$ and 3.0 m, respectively, and a borehole length of $L = 3.0$ m.



TRIF-6119-7-0

Figure 11. Dimensionless pressure contours of $(P_f - P_a)/(P_\infty - P_a)$ at a penetration depth of $D_p = 3.0$ m, for a borehole with DRZ inner and outer radii of $a = 0.05$ m and $b = 3.0$ m, respectively, and a borehole length of $L = 3.0$ m.

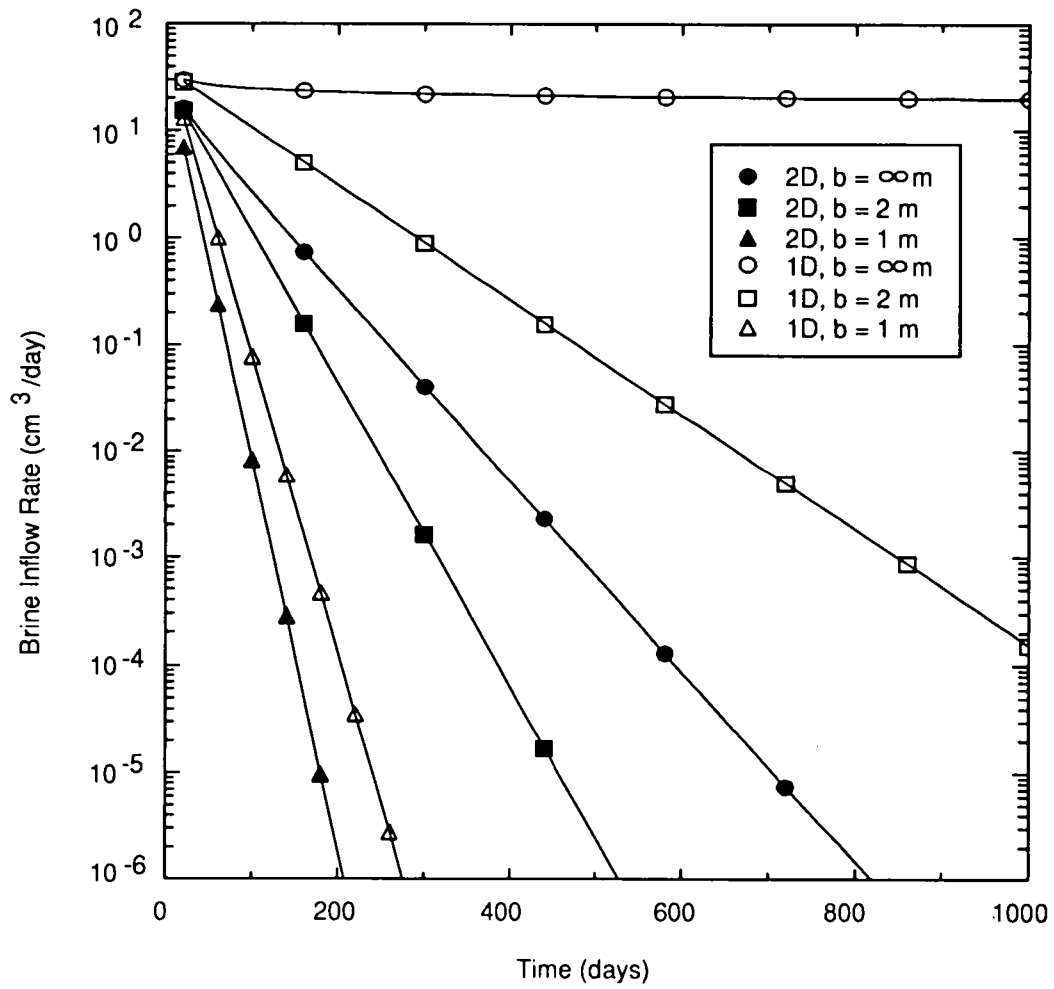
8.2 Sample Calculations of Borehole Brine Inflow Rates

The flow rate into the borehole is of greater importance than the fluid pressure in the DRZ. This rate is a readily measured quantity that can be used to estimate physical properties of the DRZ. As given in Table 2, in Figures 12, 13, and 14, brine flow rates into a borehole are shown for rock permeabilities of 10^{-20} , 10^{-21} , and 10^{-22} m^2 , respectively. Figures 16, 17, and 18 are for the same permeabilities, respectively, but for a one-year hiatus between mining the drift and drilling the borehole. The curves in these figures are calculated from Equation (6-5). To differentiate the curves, filled and unfilled symbols are used to indicate two- and one-dimensional results, respectively. The notation on the figures of 2D and 1D corresponds to two-dimensional and one-dimensional, respectively. The same symbol shape is used for results with the same DRZ outer radius. In particular, circles, squares, and triangles are used for DRZ outer radii of infinity, 2 m, and 1 m, respectively. To accommodate the wide range of flow rates, the y-axis scales in the figures are different for each figure.

Instead of analyzing individually Figures 12 to 18, to gain an understanding of the different model predictions over the range of parameters selected, it is better to discuss all four figures simultaneously. This can be accomplished by making the following seven observations given in Sections 8.2.1 to 8.2.7.

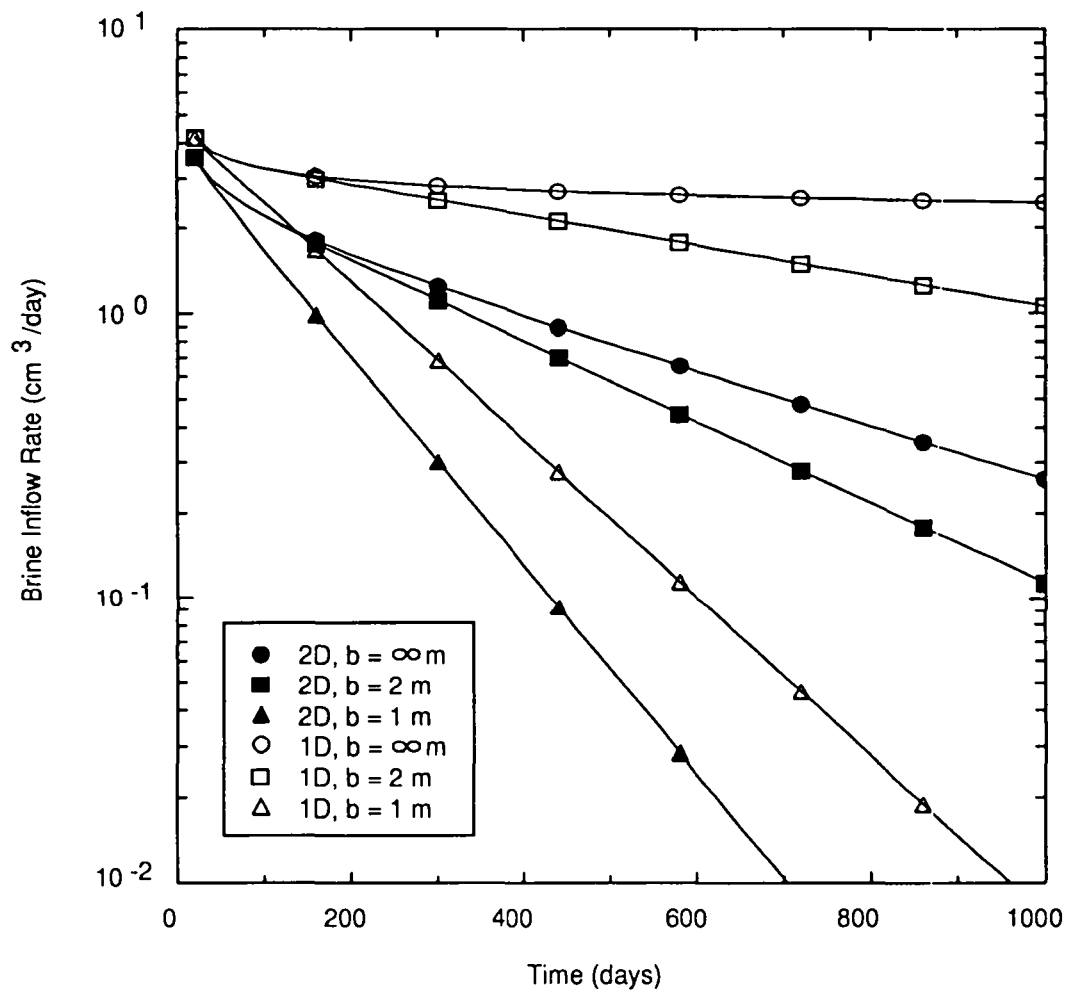
8.2.1. Flow Rate as $t \rightarrow 0$

At time just greater than zero, the fluid pressure at the borehole surface, $r = a$, is P_a , and is P_∞ for $r > a$. This discontinuity results in an infinite flow rate at time just greater than zero. To avoid this mathematical problem, the flow rates are plotted beginning with short, but nonzero times.



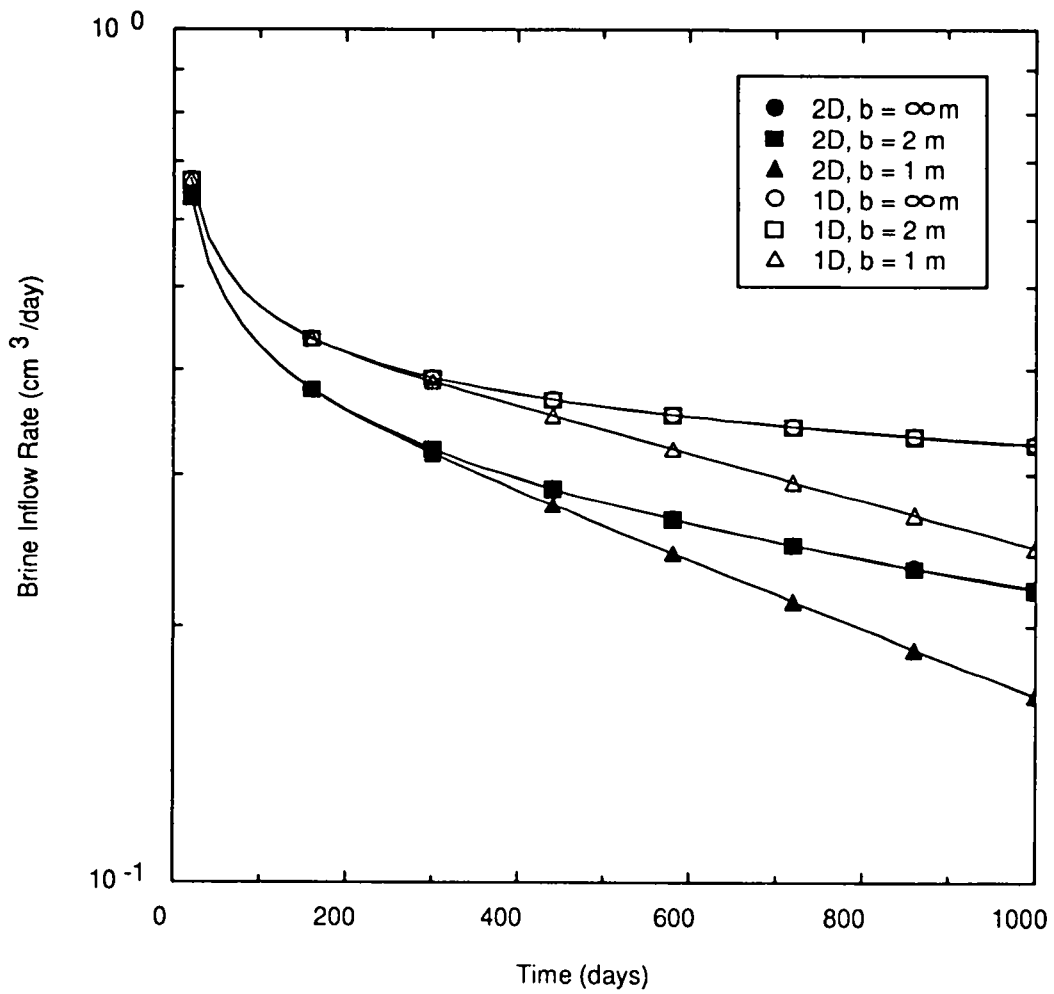
TRIf-6119-8-0

Figure 12. Brine inflow rates calculated for one- and two-dimensional models for a rock permeability of $k = 10^{-20} \text{ m}^2$.



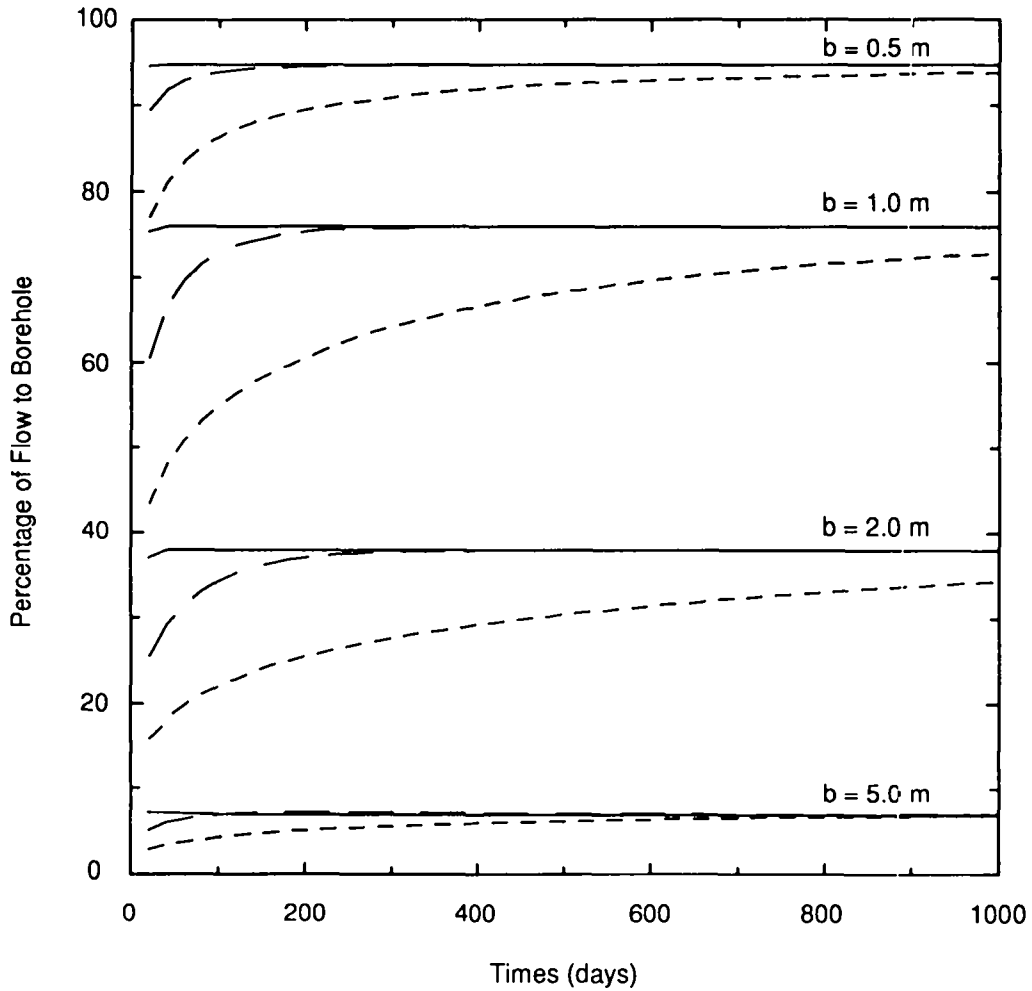
TRH-6119-9-0

Figure 13. Brine inflow rates calculated for one- and two-dimensional models for a rock permeability of $k = 10^{-21} \text{ m}^2$.



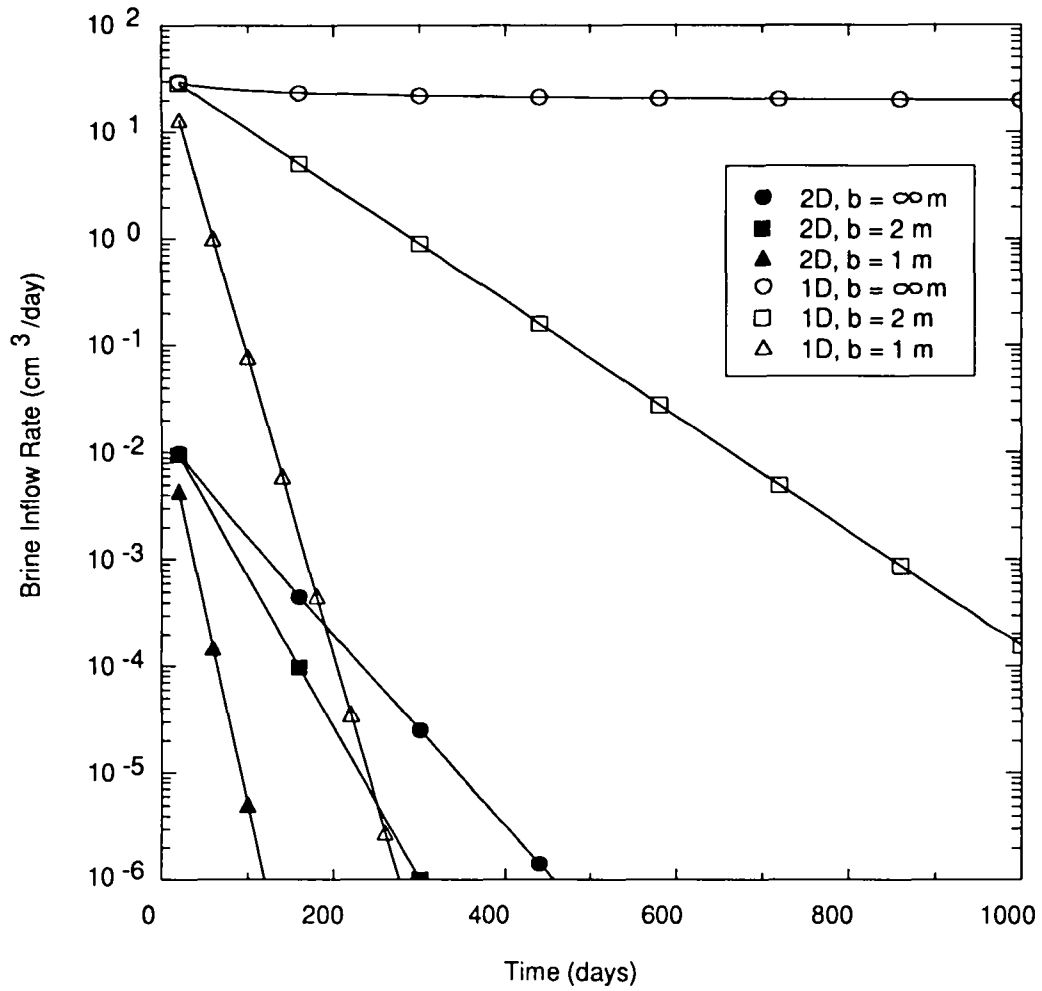
TRIF-6119-3-0

Figure 14. Brine inflow rates calculated for one- and two-dimensional models for a rock permeability of $k = 10^{-22} \text{ m}^2$.



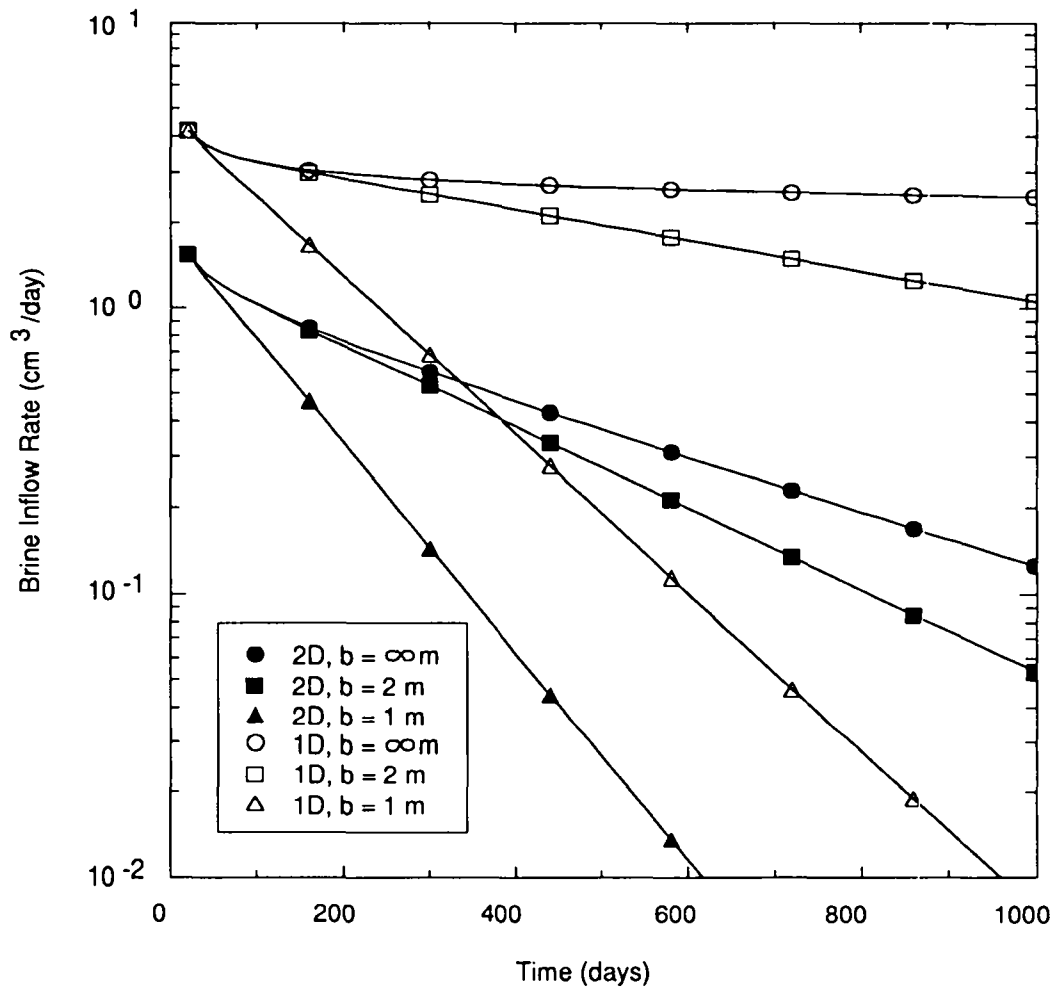
TRIF-6119-18-0

Figure 15. Percentage of flow rate to borehole for the two-dimensional model. The solid, long dash, and short dash lines are for rock permeabilities of $k = 10^{-20} \text{ m}^2$, 10^{-21} m^2 , and 10^{-22} m^2 , respectively. The asymptote for long times is given by Equation (6-15), and is independent of k .



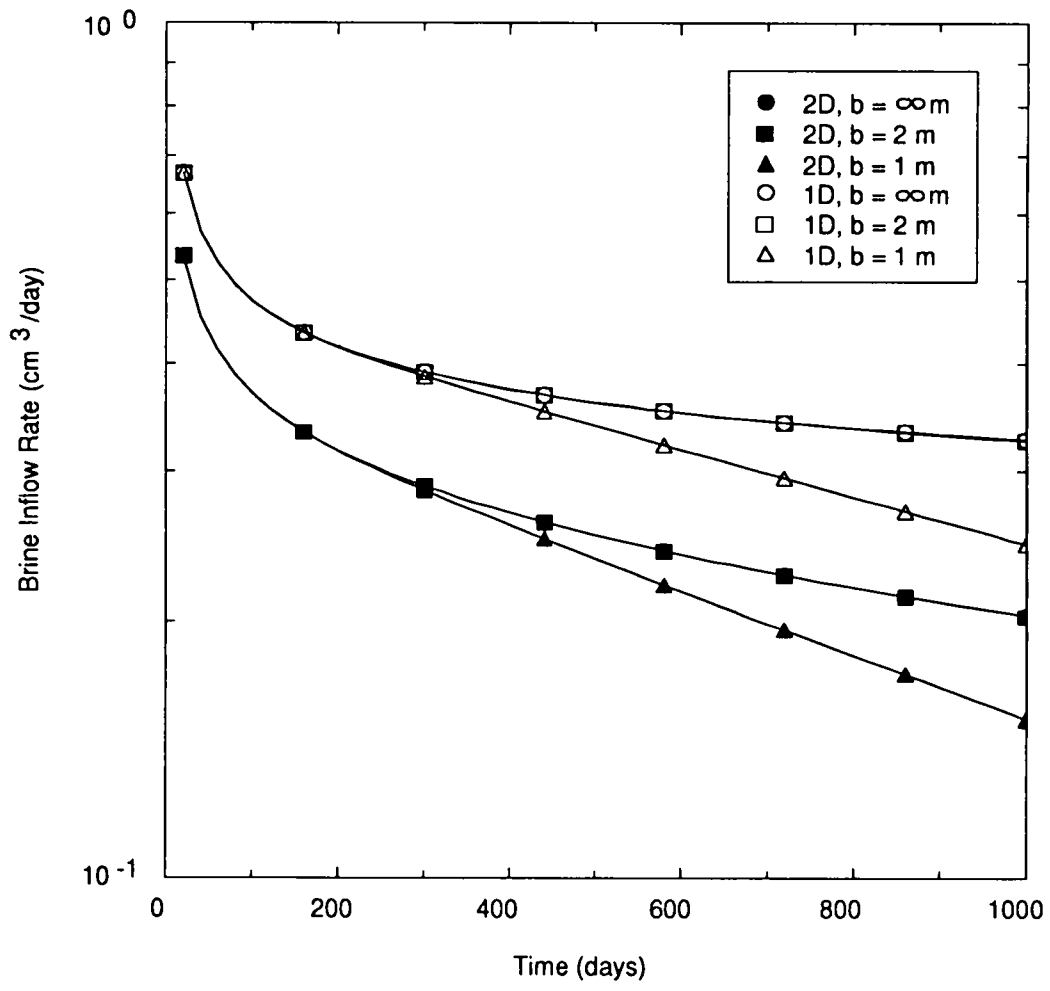
TRIF-6119-19-0

Figure 16. Brine inflow rates calculated for one- and two-dimensional models for a rock permeability of $k = 10^{-20} \text{ m}^2$. Time period between mining the drift and drilling the borehole = $\tau = 1$ year.



TRIF-6119-14-0

Figure 17. Brine inflow rates calculated for one- and two-dimensional models for a rock permeability of $k = 10^{-21} \text{ m}^2$. Time period between mining the drift and drilling the borehole = $\tau = 1$ year.



TRIF-6119-15-0

Figure 18. Brine inflow rates calculated for one- and two-dimensional models for a rock permeability of $k = 10^{-22} \text{ m}^2$. Time period between mining the drift and drilling the borehole = $\tau = 1$ year.

8.2.2. Model with Maximum Flow Rate

For the same permeability (i.e., for the same figure) and for the same DRZ outer radius, the one-dimensional solutions always have the greater flow rate. This is because flow to the drift is neglected in the one-dimensional models. Furthermore, the one-dimensional infinite-radius model always has a flow rate greater than that for the one-dimensional finite-radius model because the former has no barrier to flow at any radial distance from the borehole.

8.2.3. Flow Rate for Same Dimensionality but Varying DRZ Outer Radius

For the same dimensionality, the flow rates for the infinite-radius and finite-radius models are comparable when the penetration depth is less than the borehole length and less than the distance given by the difference in outer and inner radii of the DRZ. In this case, the finite boundary has not yet had the opportunity to affect the flow. This may be achieved by increasing the outer radius of the DRZ, and/or decreasing the permeability. Notice in Figures 12 and 13 that as the outer radius of the DRZ increases the finite-radius model flow rates are closer to the flow rates for the infinite-radius models. In Figure 14, with the lowest permeability, the finite-radius solutions with $b = 2$ m are essentially indistinguishable from solutions with the same dimensionality, but with $b \rightarrow \infty$.

8.2.4. Effects of Penetration Depth Relative to Radial Distance

As mentioned in Section 8.2.3, the penetration depth can also be decreased by decreasing the permeability. Because penetration depth varies as the square root of the permeability, the sequence of Figures 12, 13, and 14 have penetrations depths that decrease by factors of $10^{1/2} = 3.16$ for the same time given on the x-axis of the figures. For example, at 1000 days, the penetration depths in Figures 12, 13, and 14 are 17.2, 5.44, and 1.72 m, respectively. Thus, the penetration depths in Figures 12 and 13 at 1000 days are greater than the outer radius minus the inner radius of the DRZ (i.e., $D_p > b - a = 0.95$ m for $b = 1.0$ m, and $D_p > b - a = 1.95$ m for $b = 2.0$ m). Because the penetration depths are greater than the difference in radii, for

the same dimensionality the effects of a finite-radius DRZ will reduce the flow rate below that for an infinite-radius DRZ. Therefore, in Figures 12 and 13, for the same dimensionality the finite-radius model flow rates are significantly less than those of the infinite-radius model flow rates. However, in Figure 14 at 1000 days, for the same dimensionality the infinite-radius solutions are virtually indistinguishable from the finite-radius solutions with $b = 2.0$ m. In this case, the difference in DRZ radii of 1.95 m is greater than the penetration depth of 1.72 m, so the effect of a finite-radius DRZ has not yet affected the flow.

8.2.5. Conditional Test for Using One-Dimensional Models

The conditional test given by Equation (6-9) requires $[D_p/L]_* \leq 0.0886$ for the two-dimensional brine inflow rate to be within 5% of that for the one-dimensional model. From Equation (6-9), for permeabilities of $k = 10^{-20}$, 10^{-21} , and 10^{-22} m², the times for which this conditional test are satisfied are 0.239, 2.39, and 23.9 days, respectively. However, if agreement between one- and two-dimensional models need only be within 50%, then the conditional test in Equation (6-9) is satisfied for times less than 23.9, 239, and 2390 days for the same set of permeabilities, respectively. This analysis agrees with the inflow rates shown in Figures 12 to 14. In particular, note from Figure 14 that the two-dimensional brine inflow rate is always within 50% of the one-dimensional brine inflow rate. This is expected because the time period shown is less than 2390 days, as required by the conditional test given by Equation (6-9).

8.2.6. Percentage of Flow Rate to the Borehole

Because the two-dimensional model includes flow to the borehole and to the drift, it is of interest to determine F_g , the percentage of the flow rate to the borehole. As given by Equation (6-14), this percentage varies with time, permeability, and DRZ outer radius. A plot of F_g for permeabilities of $k = 10^{-20}$, 10^{-21} , and 10^{-22} m² is given in Figure 15. As shown in Figure 15, the results for long times are insensitive to the permeability and time. This agrees with Equation (6-15), in which the only parameters that determine the long-time behavior of F_g are a , b , and L . To use Equation (6-15), λ_1 and η_1 must be calculated. For example, for $b = 1.0$ m, λ_1 can be estimated

from Figure 6, or from using the technique in Appendix A to obtain a more accurate value of $\lambda_1 = 0.930 \text{ m}^{-1}$. In the sample calculations $L = 3.0 \text{ m}$, and thus according to Equation (2-26), $\eta_1 = 0.524 \text{ m}^{-1}$. Substituting these values into Equation (6-15) provides the long-time solution for $F_d = 75.9\%$ as given in Figure 15. Thus, for $b = 1.0 \text{ m}$, approximately 24% of the flow rate is to the drift for long times.

A physical explanation for the results shown in Figure 15 can be obtained by noting that the surface area of the drift floor available for fluid to escape increases quadratically with an increasing DRZ outer radius. However, the surface area of the borehole is independent of the DRZ outer radius. Therefore, as shown in Figure 15, the percentage of flow to the borehole decreases dramatically as the DRZ outer radius increases. Notice from Figure 15 that even for a DRZ outer radius of 2.0 m, which is less than the borehole length of 3.0 m, the dominant flow path is to the drift and not to the borehole.

8.2.7. Effect of Drilling Borehole One Year After Mining Drift

To demonstrate the effect of prior depressurization, in Figures 16 to 18 the brine inflow rates are shown for the condition that the time between mining the drift and drilling the borehole is one year. For convenience, in these calculations $H = 3.0 \text{ m}$. Prior depressurization is not included in the one-dimensional solutions, and therefore the one-dimensional inflow rates in Figures 16 to 18 are identical to those in Figures 12 to 14. However, for the two-dimensional models, in making the same comparisons among Figures 12 to 14 and 16 to 18, respectively, there are significant decreases in the inflow rates if prior depressurization is included. This is due to the reduction in pressure gradient and in the available fluid caused by fluid previously escaping into the drift. In comparing Figures 16 to 18, this effect decreases as the permeability decreases because less fluid has had the opportunity to escape for the same time period of one year.

9.0 CONCLUSIONS

This work presented a detailed derivation of the solutions to the Diffusion Equation in cylindrical coordinates that are applicable to modeling flow in a DRZ. The solutions apply to DRZs of arbitrary radial extent from a borehole drilled from a drift, and are useful for determining fluid pressures and borehole fluid inflow rates. The solution domain is restricted to constant homogeneous rock and fluid properties in the DRZ and pressures in the borehole and at the surface of the drift that are maintained constant at ambient conditions. These solutions remove the modeling constraints of one-dimensional radial flow for a DRZ of infinite extent, and thus provide a basis for assessing the significance of neglecting flow to the drift, both before and after drilling the borehole, and for assessing the effects of a finite DRZ. The solutions are also useful for providing benchmark test cases for more detailed numerical calculations.

Based on the solutions presented, an exact quantitative criterion was developed for assessing the importance of two-dimensional effects on the borehole brine inflow rate. This criterion provides a conditional test to determine for a specified tolerance on the agreement between the one- and two-dimensional solutions, up to what time two-dimensional effects are not important. For this initial period, the one-dimensional model may be used. For convenience, Equation (6-9) and the plot given in Figure 5 can be used to determine the maximum time that the two- and one-dimensional solutions will be comparable. This analysis assumes that the initial pressure is uniform. If the initial pressure is not uniform, such as in the case that there was much time between mining the drift and drilling the borehole, the two-dimensional model is appropriate because it includes depth-dependent variations. In this case, for long times, the ratio of the flow rate to the borehole and to the drift may be determined from Equation (6-15) and Figure 6.

Although, as given in Table 1, the two-dimensional finite-radius model presented in this work removes three of the limitations of the one-dimensional infinite-radius model, the extent of the DRZ is not determined from the model and must be specified independently. In addition, the model neglects flow up from below the DRZ.

Further work is needed to extend the two-dimensional model to include flow up from below the DRZ. For two-dimensional modeling to be practical, a direct method for estimating physical properties from fluid inflow rates is also needed. Such a method has been developed for the one-dimensional infinite-radius model (Nowak and McTigue, 1987; Nowak et al., 1988) and should be developed for two-dimensional models.

10.0 REFERENCES

- Abramowitz, M., and I. Stegun, eds. 1970. *Handbook of Mathematical Functions with Formulas, Graphs, and Mathematical Tables*. 8th printing. New York, NY: Dover Publications.
- Arpaci, V.S. 1966. *Conduction Heat Transfer*. Reading, MA: Addison-Wesley Publishing Company. 365-368.
- Carslaw, H.S., and J.C. Jaeger. 1959. *Conduction of Heat in Solids*. 2nd ed. Oxford, England: Clarendon Press.
- Crank, J. 1975. *The Mathematics of Diffusion*. 2nd ed. Oxford, England: Clarendon Press.
- Finley, S.J., D.J. Hanson, and R. Parsons. 1992. *Small-Scale Brine Inflow Experiments--Data Report Through 6/6/91*. SAND91-1956. Albuquerque, NM: Sandia National Laboratories.
- Freeze, R.A. and J.A. Cherry. 1979. *Groundwater*. Englewood Cliffs, NJ: Prentice-Hall, Inc. 65.
- Goldstein, S. 1932. "Some Two-Dimensional Problems with Circular Symmetry," *Proceedings of the London Mathematical Society*. Second Series, Vol. 34, 51-88.
- Gray, A., G.B. Mathews, and T.M. MacRoberts. 1922. *A Treatise on Bessel Functions and Their Applications to Physics*. 2nd ed. London: MacMillan and Co., Limited. 97.
- Hildebrand, F.B. 1962. *Advanced Calculus for Applications*. Englewood Cliffs, NJ: Prentice-Hall, Inc. 236-238.
- McTigue, D.F., and E.J. Nowak. 1988. "Brine Transport in the Bedded Salt of the Waste Isolation Pilot Plant (WIPP): Field Measurements and a Darcy Flow Model," *Scientific Basis for Nuclear Waste Management XI, Boston, MA*,

November 30 - December 3, 1987. Eds. M.J. Apter and R.E. Westerman. SAND87-1274C. Pittsburgh, PA: Materials Research Society. Vol. 112, 209-218.

Nicholson, J.W. 1921. "A Problem in the Theory of Heat Conduction," *Proceedings of the Royal Society of London. Series A, Vol. C*, 226-240.

Nowak, E.J., and D.F. McTigue. 1987. *Interim Results of Brine Transport Studies in the Waste Isolation Pilot Plant (WIPP)*. SAND87-0880. Albuquerque, NM: Sandia National Laboratories.

Nowak, E.J., D.F. McTigue, and R. Beraun. 1988. *Brine Inflow to WIPP Disposal Rooms: Data, Modeling, and Assessment*. SAND88-0112. Albuquerque, NM: Sandia National Laboratories.

Rechard, R.P., A.C. Peterson, J.D. Schreiber, H.J. Iuzzolino, M.S. Tierney, and J.S. Sandha, eds. 1991. *Preliminary Comparison with 40 CFR Part 191, Subpart B for the Waste Isolation Pilot Plant, December 1991. Volume 3: Reference Data*. SAND91-0893/3. Albuquerque, NM: Sandia National Laboratories. A-81.

Watson, G.N. 1958. *A Treatise on the Theory of Bessel Functions*. 2nd ed. London, England: Syndics of the Cambridge University Press.

Webb, S.W. In review. "Brine Inflow Sensitivity Studies for Waste Isolation Pilot Plant Boreholes: Results of One-Dimensional Simulations." SAND91-2296. Review copy on file at the Waste Management and Transportation Library. Albuquerque, NM: Sandia National Laboratories.

APPENDIX A: DETERMINING EIGENVALUES IN THE RADIAL DIRECTION

Appendix A: Determining Eigenvalues in the Radial Direction

The eigenvalues λ_i are determined from Equation (2-20) and are calculated numerically. In this Appendix, a simple but highly efficient Newton iteration method is presented for determining the eigenvalues.

To begin the iteration, a first guess for the eigenvalues may be obtained by using asymptotic expansions for the Bessel functions for large values of their arguments given by (Abramowitz and Stegun, 1970, p. 364, Eqs. 9.2.1 and 9.2.2)

$$J_n(x) \rightarrow \sqrt{\frac{2}{\pi x}} \cos\left[x - \frac{n\pi}{2} - \frac{\pi}{4}\right] \quad \text{as } x \rightarrow \infty \quad (\text{A-1})$$

$$Y_n(x) \rightarrow \sqrt{\frac{2}{\pi x}} \sin\left[x - \frac{n\pi}{2} - \frac{\pi}{4}\right] \quad \text{as } x \rightarrow \infty \quad (\text{A-2})$$

Using Equations (A-1) and (A-2), Equation (2-20) for the first guess of eigenvalue i , λ_i^* , reduces to

$$0 = \cos\left[\lambda_i^* b - \frac{3\pi}{4}\right] \sin\left[\lambda_i^* a - \frac{\pi}{4}\right] - \cos\left[\lambda_i^* a - \frac{\pi}{4}\right] \sin\left[\lambda_i^* b - \frac{3\pi}{4}\right] \quad (\text{A-3})$$

Solving Equation (A-3) for λ_i^* results in

$$\lambda_i^* = \frac{\pi(2i-1)}{b-a} \quad i = 1, 2, 3, \dots \quad (\text{A-4})$$

With this initial guess, the next iterate for λ_i is given by

$$\lambda_i = \lambda_i^* - \frac{g(\lambda_i^*)}{\left. \frac{dg}{d\lambda} \right|_{\lambda=\lambda_i^*}} \quad (\text{A-5})$$

where

$$g(\lambda_i^*) = Y_0(\lambda_i^* a) J_1(\lambda_i^* b) - Y_1(\lambda_i^* b) J_0(\lambda_i^* a) \quad (\text{A-6})$$

Using Equations (2-16), (2-17), and the following identities (Abramowitz and Stegun, 1970, p. 361, Eq. 9.1.30),

$$\frac{dJ_1(x)}{dx} = J_0(x) - \frac{J_1(x)}{x} \quad (\text{A-7})$$

$$\frac{dY_1(x)}{dx} = Y_0(x) - \frac{Y_1(x)}{x} \quad (\text{A-8})$$

we have that

$$\begin{aligned} \frac{dg}{d\lambda} = & a[Y_1(\lambda b)J_1(\lambda a) - J_1(\lambda b)Y_1(\lambda a)] + b[J_0(\lambda b)Y_0(\lambda a) - J_0(\lambda a)Y_0(\lambda b)] \\ & + \frac{1}{\lambda} \left[J_0(\lambda a)Y_1(\lambda b) - Y_0(\lambda a)J_1(\lambda b) \right] \quad (\text{A-9}) \end{aligned}$$

The next iterate can now be determined by substituting Equations (A-6) and (A-9) into Equation (A-5), and repeatedly using Equation (A-5) to converge to the eigenvalue.

Reference for Appendix A

Abramowitz, M., and I. Stegun, eds. 1970. *Handbook of Mathematical Functions with Formulas, Graphs, and Mathematical Tables*. 8th printing. New York, NY: Dover Publications.

APPENDIX B: EVALUATING INTEGRAL FOR AN INFINITE RADIAL DOMAIN

Appendix B: Evaluating Integral for an Infinite Radial Domain

Approximations of the integral obtained for infinite-domain problems have been reported (Jaeger, 1942; Jaeger and Clarke, 1942). A convenient method developed by D.F. McTigue (Sandia National Laboratories, Department 1513) to evaluate the first part of the integrals in Equation (6-5) may be derived by substituting $\beta = a\lambda$ so that

$$I(0, \epsilon) = \int_0^{\epsilon} \frac{e^{-\alpha\lambda^2 t}}{\lambda [J_0^2(\lambda a) + Y_0^2(\lambda a)]} d\lambda \quad \text{as } \epsilon \rightarrow 0 \quad (\text{B-1})$$

becomes

$$I(0, \epsilon) = \int_0^{\epsilon a} \frac{e^{-\alpha\beta^2 t/a^2}}{\beta [J_0^2(\beta) + Y_0^2(\beta)]} d\beta \quad \text{as } \epsilon \rightarrow 0 \quad (\text{B-2})$$

As $\beta \rightarrow 0$, the asymptotics (Abramowitz and Stegun, 1970, p. 360, Eqs. 9.1.12 and 9.1.13)

$$J_0(\beta) \rightarrow 1 - \frac{\beta^2}{4} + \dots \quad \text{as } \beta \rightarrow 0 \quad (\text{B-3})$$

$$Y_0(\beta) \rightarrow \frac{2}{\pi} \left[\ln \left[\frac{\beta e^{\gamma}}{2} \right] \right] J_0(\beta) + \dots \quad \text{as } \beta \rightarrow 0 \quad (\text{B-4})$$

can be used to simplify the denominator of the integrand in Equation (B-2) so that

$$I(0, \varepsilon) = \frac{\pi^2}{4} \int_0^{\varepsilon a} \frac{e^{-\alpha\beta^2 t/a^2}}{\beta \left(\ln \left[\frac{\beta e^\gamma}{2} \right] \right)^2} d\beta \quad \text{as } \varepsilon a \rightarrow 0 \quad . \quad (\text{B-5})$$

Integrating Equation (B-5) by parts results in

$$I(0, \varepsilon) = \frac{\pi^2}{4} \left\{ \frac{e^{-\alpha\varepsilon^2 t}}{\ln \left[\frac{\varepsilon a e^\gamma}{2} \right]} + \text{higher order terms} \right\} \quad \text{as } \varepsilon a \rightarrow 0 \quad . \quad (\text{B-6})$$

The second part of the infinite-domain integral is given by

$$I(\varepsilon, \infty) = \int_{\varepsilon}^{\infty} \frac{e^{-\alpha\lambda^2 t}}{\lambda \left[J_0^2(\lambda a) + Y_0^2(\lambda a) \right]} d\lambda \quad \varepsilon > 0 \quad , \quad (\text{B-7})$$

which may be evaluated numerically because there are no singularities in the integrand for $\varepsilon > 0$.

References for Appendix B

Abramowitz, M., and I. Stegun, eds. 1970. *Handbook of Mathematical Functions with Formulas, Graphs, and Mathematical Tables*. 8th printing. New York, NY: Dover Publications.

Jaeger, J.C. 1942. "Heat Flow in the Region Bounded Internally by a Circular Cylinder," *Proceedings of the Royal Society of Edinburgh*. Section A, Vol. 61, pt. 3, 223-228.

Jaeger, J.C. and M. Clarke. 1942. "A Short Table of

$\int_0^{\infty} \exp(-xu^2) / [J_0^2(u) + Y_0^2(u)] u \, du,$ " *Proceedings of the Royal Society of Edinburgh*. Section A, Vol. 61, pt. 3, 223-228.

DISTRIBUTION

Federal Agencies

US Department of Energy, (5)
Office of Civilian Radioactive Waste
Management

Attn: Deputy Director, RW-2
Associate Director, RW-10
Office of Program
Administration and
Resources Management
Associate Director, RW-20
Office of Facilities
Siting and Development
Associate Director, RW-30
Office of Systems
Integration and
Regulations
Associate Director, RW-40
Office of External
Relations and Policy

Forrestal Building
Washington, DC 20585

US Department of Energy (4)
WIPP Project Integration Office

Attn: W.J. Arthur III
L.W. Gage
P.J. Higgins
D.A. Olona
PO Box 5400
Albuquerque, NM 87115-5400

US Department of Energy
Attn: National Atomic Museum Library
Albuquerque Operations Office
PO Box 5400
Albuquerque, NM 87185-5400

US Department of Energy (4)
WIPP Project Site Office (Carlsbad)

Attn: R. Becker
V. Daub
J. Lippis
J.A. Mewhinney
PO Box 3090
Carlsbad, NM 88221

US Department of Energy
Research & Waste Management Division
Attn: Director
PO Box E
Oak Ridge, TN 37831

US Department of Energy
Attn: E. Young
Room E-178
GAO/RCED/GTN
Washington, DC 20545

US Department of Energy
Office of Environmental Restoration
and Waste Management
Attn: J. Lytle, EM-30 (Trevion II)
Washington, DC 20585-0002

US Department of Energy (3)
Office of Environmental Restoration
and Waste Management
Attn: M. Frei, EM-34 (Trevion II)
Washington, DC 20585-0002

US Department of Energy
Office of Environmental Restoration
and Waste Management
Attn: S. Schneider, EM-342
(Trevion II)
Washington, DC 20585-0002

US Department of Energy (3)
Office of Environment, Safety
and Health
Attn: C. Borgstrom, EH-25
R. Pelletier, EH-231
Washington, DC 20585

US Department of Energy (2)
Idaho Operations Office
Fuel Processing and Waste
Management Division
785 DOE Place
Idaho Falls, ID 83402

US Environmental Protection
Agency (2)
Radiation Programs (ANR-460)
Attn: R. Guimond
Washington, DC 20460

US Geological Survey (2)
Water Resources Division
Attn: R. Livingston
Suite 200
4501 Indian School, NE
Albuquerque, NM 87110

US Nuclear Regulatory Commission
Attn: H. Marson
Mail Stop 623SS
Washington, DC 20555

Boards

Defense Nuclear Facilities Safety
Board
Attn: D. Winters
Suite 700
625 Indiana Ave., NW
Washington, DC 20004

Nuclear Waste Technical Review
Board (2)
Attn: D.A. Deere
S.J.S. Parry
Suite 910
1100 Wilson Blvd.
Arlington, VA 22209-2297

Advisory Committee on Nuclear Waste
Nuclear Regulatory Commission
Attn: R. Major
7920 Norfolk Ave.
Bethesda, MD 20814

State Agencies

Environmental Evaluation Group (3)
Attn: Library
Suite F-2
7007 Wyoming, NE
Albuquerque, NM 87109

NM Bureau of Mines and Mineral
Resources
Socorro, NM 87801

NM Energy, Minerals, and Natural
Resources Department
Attn: Library
2040 S. Pacheco
Santa Fe, NM 87505

NM Environment Department (3)
Secretary of the Environment
Attn: J. Espinosa
1190 St. Francis Drive
Santa Fe, NM 87503-0968

NM Environment Department
WIPP Project Site
Attn: P. McCasland
PO Box 3090
Carlsbad, NM 88221

Laboratories/Corporations

Battelle Pacific Northwest
Laboratories (2)
Attn: H.C. Burkholder, P7-41
R.E. Westerman, P8-37
Battelle Blvd.
Richland, WA 99352

INTERA Inc.
Attn: J.F. Pickens
Suite 300
6850 Austin Center Blvd.
Austin, TX 78731

INTERA Inc.
Attn: W. Stensrud
PO Box 2123
Carlsbad, NM 88221

IT Corporation
Attn: R.F. McKinney
Regional Office - Suite 700
5301 Central, NE
Albuquerque, NM 87108

Los Alamos National Laboratory
Attn: B. Erdal, CNC-11
PO Box 1663
Los Alamos, NM 87544

RE/SPEC, Inc.
Attn: W. Coons
Suite 300
4775 Indian School, NE
Albuquerque, NM 87110-3927

RE/SPEC, Inc.
Attn: J.L. Ratigan
PO Box 725
Rapid City, SD 57709

Savannah River Laboratory (3)
Attn: N. Bibler
M.J. Plodinec
G.G. Wicks
Aiken, SC 29801

Southwest Research Institute (2)
Center for Nuclear Waste
Regulatory Analysis
Attn: P.K. Nair
6220 Culebra Road
San Antonio, TX 78223-0510

SAIC

Attn: G. Dymmel
101 Convention Center Dr.
Las Vegas, NV 89109

SAIC

Attn: H.R. Pratt,
10260 Campus Point Dr.
San Diego, CA 92121

SAIC (2)

Attn: M. Davis
J. Tollison
2109 Air Park Rd., SE
Albuquerque, NM 87106

Tech Reps Inc. (3)

Attn: J. Chapman
R. Jones
E. Lorusso
5000 Marble, NE
Albuquerque, NM 87110

Westinghouse Electric Corporation (5)

Attn: Library
C. Cox
L. Fitch
R. Kehrman
L. Trego
PO Box 2078
Carlsbad, NM 88221

Universities

University of New Mexico
Geology Department
Attn: Library
Albuquerque, NM 87131

University of Washington
Attn: G.R. Heath
College of Ocean
and Fishery Sciences
583 Henderson Hall
Seattle, WA 98195

Individuals

P. Drez
8816 Cherry Hills Rd., NE
Albuquerque, NM 87111

D.W. Powers
Star Route Box 87
Anthony, TX 79821

Libraries

Thomas Brannigan Library

Attn: D. Dresp
106 W. Hadley St.
Las Cruces, NM 88001

Government Publications Department
General Library

University of New Mexico
Albuquerque, NM 87131

Hobbs Public Library

Attn: M. Lewis
509 N. Ship St.
Hobbs, NM 88248

New Mexico Junior College

Pannell Library
Attn: R. Hill
Lovington Highway
Hobbs, NM 88240

New Mexico State Library

Attn: N. McCallan
325 Don Gaspar
Santa Fe, NM 87503

New Mexico Tech

Martin Speere Memorial Library
Campus Street
Socorro, NM 87810

WIPP Public Reading Room

Carlsbad Public Library
Attn: Director
101 S. Halagueno St.
Carlsbad, NM 88220

**National Academy of Sciences,
WIPP Panel**

Charles Fairhurst, Chairman
Department of Civil and
Mineral Engineering
University of Minnesota
500 Pillsbury Dr., SE
Minneapolis, MN 55455-0220

Howard Adler
Oak Ridge Associated Universities
Medical Sciences Division
PO Box 117
Oak Ridge, TN 37831-0117

Ina Alterman
Board on Radioactive
Waste Management
GF456
2101 Constitution Ave.
Washington, DC 20418

John D. Bredehoeft
Western Region Hydrologist
Water Resources Division
US Geological Survey (M/S 439)
345 Middlefield Road
Menlo Park, CA 94025

Fred M. Ernsberger
250 Old Mill Road
Pittsburgh, PA 15238

Rodney C. Ewing
Department of Geology
University of New Mexico
Albuquerque, NM 87131

B. John Garrick
PLG, Inc.
Suite 400
4590 MacArthur Blvd.
Newport Beach, CA 92660-2027

Leonard F. Konikow
US Geological Survey
431 National Center
Reston, VA 22092

Peter B. Myers
National Academy of Sciences
Board on Radioactive
Waste Management
2101 Constitution Ave.
Washington, DC 20418

Jeremiah O'Driscoll
Jody Incorporated
505 Valley Hill Drive
Atlanta, GA 30350

Christopher G. Whipple
Clement International
Suite 1380
160 Spear St.
San Francisco, CA 94105

Foreign Addresses

Studiecentrum Voor Kernenergie
Centre D'Energie Nucleaire
Attn: A. Bonne
SCK/CEN
Boeretang 200
B-2400 Mol, BELGIUM

Atomic Energy of Canada, Ltd. (3)
Whiteshell Research Estab.
Attn: B. Goodwin
M. Stevens
D. Wushke
Pinewa, Manitoba, CANADA R0E 1L0

Francois Chenevier, Director (2)
ANDRA
Route du Panorama Robert Schumann
B.P.38
92266 Fontenay-aux-Roses Cedex
FRANCE

Jean-Pierre Olivier
OECD Nuclear Energy Agency
Division of Radiation Protection
and Waste Management
38, Boulevard Suchet
75016 Paris, FRANCE

Claude Sombret
Centre D'Etudes Nucleaires
De La Vallee Rhone
CEN/VALRHO
S.D.H.A. BP 171
30205 Bagnols-Sur-Ceze, FRANCE

Bundesministerium fur Forschung und
Technologie
Postfach 200 706
5300 Bonn 2, GERMANY

Gesellschaft fur Reaktorsicherheit
(GRS) (2)
Attn: B. Baltes
W. Muller
Schwertnergasse 1
D-5000 Cologne, GERMANY

Bundesanstalt fur Geowissenschaften
und Rohstoffe
Attn: M. Langer
Postfach 510 153
3000 Hanover 51, GERMANY

Hahn-Meitner-Institut für
Kernforschung
Attn: W. Lutze
Glienicke Strasse 100
100 Berlin 39, GERMANY

Institut für Tieflagerung (2)
Attn: K. Kuhn
Theodor-Heuss-Strasse 4
D-3300 Braunschweig, GERMANY

Physikalisch-Technische Bundesanstalt
Attn: P. Brenneke
Postfach 3345
D-3300 Braunschweig, GERMANY

Shingo Tashiro
Japan Atomic Energy Research Inst.
Tokai-Mura, Ibaraki-Ken, 319-11
JAPAN

S Majid Hassanizadeh
Senior Scientific Researcher
Soil and Groundwater Research
National Institute of Public Health
and Environmental Protection
Antonie van Leeuwenhoeklaan 9
PO Box 1
3720 BA BILTHOVEN
THE NETHERLANDS

Netherlands Energy Research
Foundation ECN
Attn: L.H. Vons
3 Westerduinweg
PO Box 1
1755 ZG Petten, THE NETHERLANDS

Svensk Kärnbränsleforsörjning AB
Attn: F. Karlsson
Project KBS
Kärnbränslesakerhet
Box 5864
10248 Stockholm, SWEDEN

Nationale Genossenschaft für die
Lagerung Radioaktiver Abfälle (2)
Attn: S. Vomvoris
P. Zuidema
Hardstrasse 73
CH-5430 Wettingen, SWITZERLAND

D.R. Knowles
British Nuclear Fuels, plc
Risley, Warrington, Cheshire WA3 6AS
1002607 UNITED KINGDOM

AEA Technology
Attn: J.H. Rees
D5W/29 Culham Laboratory
Abingdon, Oxfordshire OX14 3DB
UNITED KINGDOM

AEA Technology
Attn: W.R. Rodwell
O44/A31 Winfrith Technical Centre
Dorchester, Dorset DT2 8DH
UNITED KINGDOM

AEA Technology
Attn: J.E. Tinson
B4244 Harwell Laboratory
Didcot, Oxfordshire OX11 0RA
UNITED KINGDOM

Sandia Internal

1502	J.C. Cummings
1513	D.F. McTigue
6000	D.L. Hartley
6100	R.W. Lynch
6119	E.D. Gorham
6119	F. Gelbard (15)
6119	Staff (14)
6121	J.R. Tillerson
6121	Staff (7)
6300	D.E. Miller
6302	T.E. Blejwas, Acting
6303	W.D. Weart
6303	S.Y. Pickering
6331	S.H. Conrad
6331	N.E. Olague
6341	A.L. Stevens
6341	Staff (6)
6341	WIPP Central Files (10)
6342	D.R. Anderson
6342	Staff (20)
6343	T.M. Schultheis
6343	Staff (2)
6345	R.C. Lincoln
6345	Staff (9)
6347	D.R. Schafer
9300	J.E. Powell
8523-2	Central Technical Files
7141	Technical Library (5)
7151	Technical Publications
7613-2	Document Processing for DOE/OSTI (10)

THIS PAGE INTENTIONALLY LEFT BLANK